Iterative expansion microscopy

Jae-Byum Chang[1,2], Fei Chen[3], Young-Gyu Yoon[1,4], Erica E Jung[1], Hazen Babcock[5], Jeong Seuk Kang[6], Shoh Asano[1], Ho-Jun Suk[7], Nikita Pak[8], Paul W Tillberg[4], Asmamaw T Wassie[3], Dawen Cai[9] & Edward S Boyden[1,3,10,11]

We recently developed a method called expansion microscopy, in which preserved biological specimens are physically magnified by embedding them in a densely crosslinked polyelectrolyte gel, anchoring key labels or biomolecules to the gel, mechanically homogenizing the specimen, and then swelling the gel–specimen composite by ~4.5× in linear dimension. Here we describe iterative expansion microscopy (iExM), in which a sample is expanded ~20×. After preliminary expansion a second swellable polymer mesh is formed in the space newly opened up by the first expansion, and the sample is expanded again. iExM expands biological specimens ~4.5 × 4.5, or ~20×, and enables ~25-nm-resolution imaging of cells and tissues on conventional microscopes. We used iExM to visualize synaptic proteins, as well as the detailed architecture of dendritic spines, in mouse brain circuitry.

We recently discovered that preserved biological specimens that are embedded in a swellable polymer gel with key biomolecules or labels anchored to the gel and then mechanically homogenized could be isotropically swelled ~4.5× in linear dimension by immersion in water—a process we call expansion microscopy (ExM)[1]. Since our original paper on ExM, we have developed variants that anchor proteins or RNA directly to the gel, enabling application to diverse scientific and clinical contexts[2,3]. However, all ExM variants published to date expand biological specimens by ~4.5× in linear dimension, resulting in an effective resolution for an ~300-nm diffraction-limited objective lens of ~60–70 nm (~300/4.5), which led us to ask the question of whether expansion factors greater than ~4.5× might be possible, which in turn could lead to still better resolution.

In our original ExM protocol[1], biological molecules of interest were first labeled with a primary antibody and then by a secondary antibody bearing an oligonucleotide. Then, a second oligonucleotide bearing a gel-anchoring moiety (a 5′ acrydite group) and a fluorophore was applied and anchored to a swellable polyelectrolyte gel synthesized evenly throughout the specimen. After mechanical homogenization with strong protease treatment, the polymer–specimen composite could then be expanded in water[1]. Expanding a gel >4.5-fold was possible[1] but resulted in fragile gels. We here explored whether it would be possible to synthesize, postexpansion, a second gel that could expand the specimen further and still provide sufficient mechanical support (**Fig. 1a**–**e**). To develop such an iterative ExM (iExM) protocol, we had to transfer the information (i.e., the anchored fluorophores, antibodies, or biomolecules) from the first gel to the second, disrupt the first gel, and expand the second gel.

RESULTS

Design of iterative expansion microscopy chemistry

We implemented iExM by first taking a sample and expanding it using ExM as in our original paper[1], but we applied the second oligonucleotide (green in **Fig. 1f**) without a fluorophore and used a cleavable crosslinker (e.g., the commercially available crosslinker N,N′-(1,2-dihydroxyethylene) bisacrylamide (DHEBA), whose diol bond can be cleaved at high pH[4]) for gel synthesis (**Fig. 1g**). We then embedded the expanded sample in an uncharged polyacrylamide gel prepared with a cleavable crosslinker (the re-embedding gel[3]) so that the sample could be held in the expanded state during subsequent steps. Importantly, this re-embedding gel allowed us to apply a third oligonucleotide (**Fig. 1h**), bearing a gel-anchoring moiety and fluorophore, which hybridized to the oligonucleotide anchored to the first polymer. We then formed a second polyacrylate gel, made with a conventional crosslinker (e.g., N,N′-methylenebis(acrylamide) (BIS)), which incorporated the third oligonucleotide (and thus the fluorophore, **Fig. 1i**), and then we dissolved the original gels by cleaving their crosslinkers before expanding the fluorophores away from each other through immersion in water (**Fig. 1j**). iExM typically resulted in expansion ratios of ~4.5–5.5× in the first round and ~4× in the second round for a total increase of ~16–22× (see **Supplementary Note 1** for details). In addition to this implementation of iExM, we explored using the re-embedding gel as the final gel and hydrolyzing the side groups at high pH into carboxyl groups[5] (dissolving the first gel's crosslinkers simultaneously), a process we call 'high pH' iExM (hp-iExM). hp-iExM resulted in

[1]Media Lab, Massachusetts Institute of Technology (MIT), Cambridge, Massachusetts, USA. [2]Department of Biomedical Engineering, Sungkyunkwan University, Suwon, Korea. [3]Department of Biological Engineering, MIT, Cambridge, Massachusetts, USA. [4]Department of Electrical Engineering and Computer Science, MIT, Cambridge, Massachusetts, USA. [5]Harvard Center for Advanced Imaging, Harvard University, Cambridge, Massachusetts, USA. [6]John A. Paulson School of Engineering and Applied Sciences, Harvard University, Cambridge, Massachusetts, USA. [7]Harvard-MIT Division of Health Sciences and Technology, MIT, Cambridge, Massachusetts, USA. [8]Department of Mechanical Engineering, MIT, Cambridge, Massachusetts, USA. [9]Department of Cell and Developmental Biology, Medical School, Biophysics Research Division, LS&A, University of Michigan, Ann Arbor, Michigan, USA. [10]McGovern Institute, MIT, Cambridge, Massachusetts, USA. [11]Department of Brain and Cognitive Sciences, MIT, Cambridge, Massachusetts, USA. Correspondence should be addressed to E.S.B. (esb@media.mit.edu).

RECEIVED 4 SEPTEMBER 2016; ACCEPTED 20 MARCH 2017; PUBLISHED ONLINE 17 APRIL 2017; DOI:10.1038/NMETH.4261

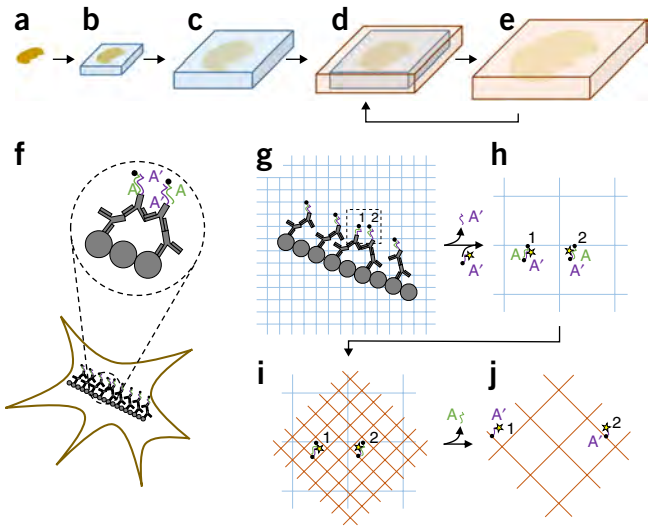

Figure 1 | Iterative expansion microscopy (iExM) concept. (**a**–**e**) Schematic of iterative expansion. (**b**) First, a swellable polyelectrolyte gel network containing a cleavable crosslinker is formed throughout a specimen, then (**c**) it is mechanically homogenized and expanded. (**d**) After expansion, a second swellable polyelectrolyte gel network is formed throughout the first, and then (**e**) it is expanded after dissolving the first gel. (**f**–**j**) Molecular view of the iExM process. (**f**) Biomolecules of interest (gray circles) are first labeled with a primary antibody (shown also in gray) followed by a secondary antibody conjugated to a DNA (purple, sequence A′) molecule, then a complementary DNA (green, sequence A) bearing a gel-anchoring moiety (acrydite, black dot), as in our original ExM procedure[1]. (**g**) The sample (two example biomolecules are labeled "1" and "2," to be followed throughout subsequent diagram panels) is embedded in a cleavable swellable polyelectrolyte gel (blue mesh). This gel incorporates the DNA of sequence A at the gel-anchoring site, and it is expanded. (**h**) A DNA oligo with the original A′ sequence (purple strand) bearing a fluorophore (yellow star) and a new gel-anchoring moiety (acrydite, black dot) is hybridized to the anchored A-sequence DNA (green). (**i**) A second swellable gel (orange mesh) is formed that incorporates the final fluorophore-bearing DNA oligo (sequence A′, purple). (**j**) The gel expands the labels away from each other after digesting the first and re-embedding gel through crosslinker cleavage.

expansion ratios slightly smaller than those of iExM (**Supplementary Note 1**), so in the main text we focus on iExM.

Validation of iterative expansion microscopy resolution and distortion

To validate iExM, we imaged the configuration of biomolecules of known organization, analyzing both the resolution obtained as well as distortion over various length scales. We analyzed microtubules, hollow tubes with an outer diameter of ~25 nm as determined by transmission electron microscopy (TEM)[6], on account of their small size and stereotyped appearance in BS-C-1 cells (**Fig. 2a**, upper left). When imaged with stochastic optical reconstruction microscopy (STORM), hollow microtubule structures were clearly resolved (**Fig. 2a**, lower right; **Fig. 2b**). When the cross-section was fit with a sum of Gaussians, the peak-to-peak distance between the sidewalls was 37.3 ± 4.7 nm (mean ± s.d. throughout; **Fig. 2c**), similar to that of previous super-resolution microscopy studies[7,8]. When these cells were expanded via iExM (**Fig. 2d,e**; ~20× physical magnification), such hollow structures could be resolved with confocal microscopy (or widefield microscopy; **Supplementary Fig. 1a**), which was not possible with earlier ~4.5× expansion factor forms of ExM[1]. For iExM-expanded samples, the average distance between the sidewall peaks was 58.7 ± 10.3 nm (**Fig. 2f**; see **Supplementary Fig. 1b**–**d** for cells processed by hp-iExM). In 3D confocal z-stacks of such cells (see **Fig. 2g** for a single *xy*-plane image and **Fig. 2h** for a single *yz*-plane image reconstructed from the z-stack image shown in **Fig. 2g**), tubular cross-sections of microtubules could easily be seen and characterized (**Fig. 2i**).

To understand the peak-to-peak distances measured by iExM versus those measured by STORM, we took into account the size of the probes used to stain the microtubules in each case. We simulated iExM images of microtubules labeled with DNA-conjugated secondary antibodies (description of simulation in **Supplementary Fig. 2** and **Supplementary Note 2**; simulator code contained in **Supplementary Software**). Using this software, we calculated the inner and outer radii of a cylinder that would contain the ends of DNA oligonucleotides borne by secondary antibodies (**Supplementary Fig. 2**; see **Supplementary Fig. 3** for a sketch of how a typical microtubule equipped with antibodies and DNA might appear). We calculated that the DNA-equipped antibodies of iExM may shift the appearance of target proteins up to ~4.6 nm relative to the position that would be obtained via classical super-resolution microscopy using antibodies lacking DNA (modeled in **Supplementary Fig. 4**; see also **Supplementary Note 3**). Such positional errors could be reduced in the future by using different DNA–antibody conjugation strategies (schematized in **Supplementary Fig. 5**; see also **Supplementary Note 4**).

Using these models, we quantitatively estimated the resolution of the overall iExM process. First, we measured the full width at half maximum (FWHM) of single microtubule sidewalls, deriving a value of 25.8 ± 7.7 nm for the point-spread function (PSF) of the overall iExM process, from staining to gelation and expansion to optical imaging (**Supplementary Fig. 6a**). To attempt to estimate the resolution of the iExM process independent of the label (e.g., focusing on the optical, gelation and expansion components), we deconvolved actual images of microtubule sidewalls by a simulated structure of an idealized DNA–antibody-labeled microtubule sidewall (generated according to the model of **Supplementary Fig. 3**), resulting in the slightly smaller value of 22.3 ± 5.3 nm (**Supplementary Fig. 6b**). Finally, we attempted to isolate just the amount of PSF broadening caused by the gelation and expansion steps specifically. We simulated (**Supplementary Fig. 6a**) how microtubules would be expected to look after staining and optical imaging, assuming that gelation and expansion induced zero error. The resultant PSF was ~6 nm smaller than the actual PSF obtained for the entire iExM process, which suggested that the processes of forming and expanding the multiple gels involved in iExM introduced ~6 nm of additional resolution error, beyond the effects of the antibodies, DNA, and optics (see **Supplementary Note 5**). Such a PSF broadening does not greatly alter the mean peak-to-peak distance between target proteins arranged in a complex (**Supplementary Fig. 6c**), but instead it widens the appearance of small proteins or protein complexes via broadening the PSF of iExM.

In ExM, physical expansion occurs in axial as well as in lateral directions, and thus ExM magnifies specimens along the optical axis as well as in the focal plane[1]. When a *yz*-plane (**Fig. 2h**) was reconstructed from the z-stack image shown in **Figure 2g**, the circular cross-section of a microtubule was resolvable

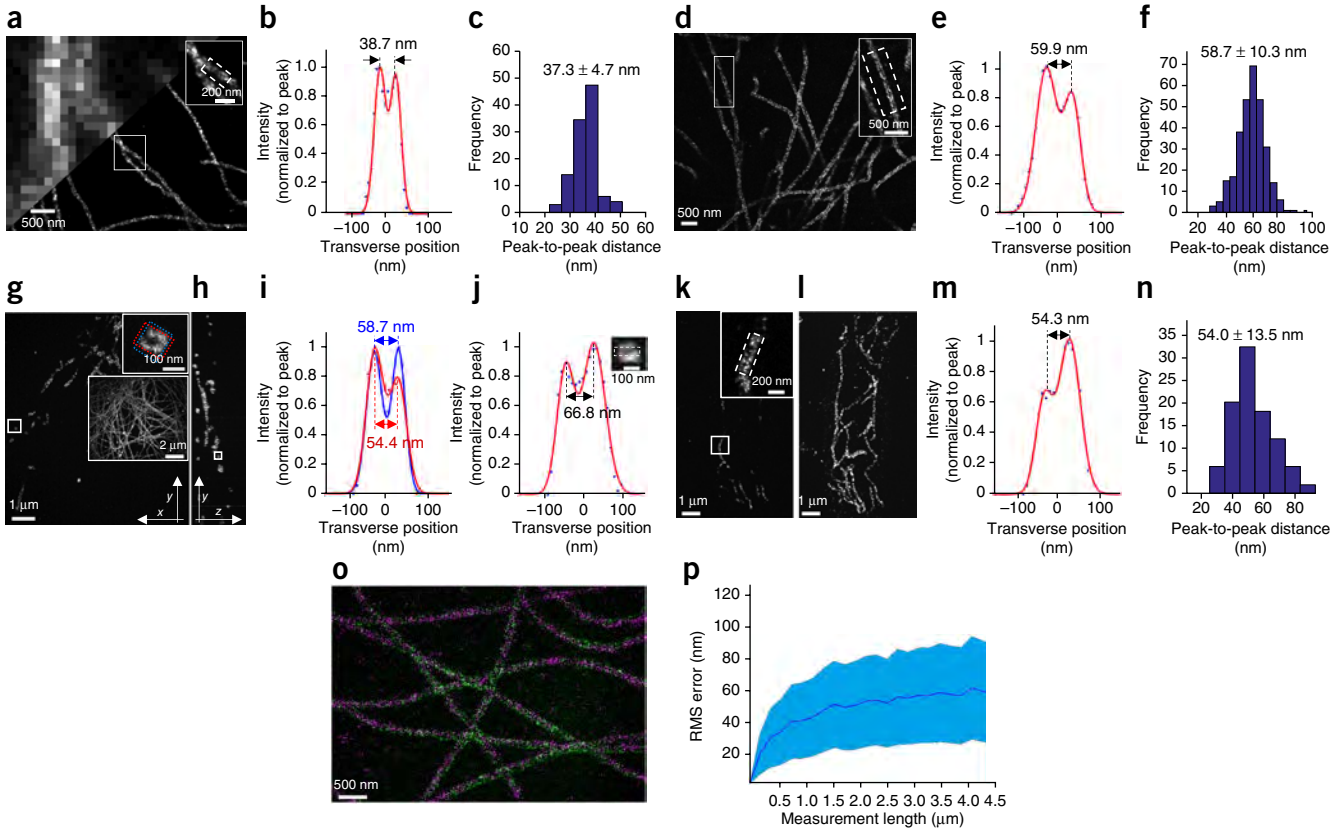

Figure 2 | Validation of the nanoscale precision of iterative expansion microscopy. (**a**–**c**) STORM imaging of cultured BS-C-1 cells after microtubules were labeled with an antitubulin antibody. (**a**) Epifluorescence image (upper left) and STORM image (lower right) of microtubules before expansion. The inset in upper right zooms in on the small box at center. (**b**) Transverse profile of microtubules in the boxed region (dotted lines) of the inset in **a** after averaging down the long axis of the box and then normalizing to the peak value (blue dots), with superimposed fit with a sum of two Gaussians (red lines). (**c**) Population data for 110 microtubule segments from two samples (mean ± s.d.), showing a histogram of peak-to-peak distances. (**d**–**j**) Confocal imaging of cultured BS-C-1 cells with labeled microtubules after ~20-fold expansion via iExM. (**d**) Single *xy*-plane image at the bottom of the cell. The inset in upper right zooms in on the small box at left. (**e**) As in **b**, but for the inset of **d**. (**f**) As in **c**, but for iExM-processed BS-C-1 cells. *n* = 307 microtubule segments from one expanded sample. (**g**) Single *xy*-plane image 1.6 µm above the bottom of the cell. The inset in upper right zooms in on the small box indicated at left, highlighting the circular cross-section of the microtubule (blue and red boxes are used to calculate the profile of **i**). The large inset at right shows the entire cellular context as a maximum intensity projection of the sample. (**h**) Single *yz*-plane within the volume imaged in **g**; the small box is highlighted in the inset of **j**. (**i**) Transverse profiles (i.e., plotting along the long axis of the highlighting box) of the microtubule in the upper right inset of **g**, with color corresponding to that of the highlighting box in the inset. (**j**) Transverse profile of the microtubule in the small box of **h**. Inset, zoomed-in image of the box of **h**, showing the cross-section of the microtubule being resolved along the optical axis. (**k**) Confocal image of a 100-µm-thick slice of mouse cortex with microtubules labeled after ~18-fold expansion via iExM, imaged at a single *xy*-plane. (**l**) Maximum intensity projection of the sample shown in **k**. (**m**) As in **e**, but for the inset of **k**. (**n**) Population data for 96 microtubule segments from one expanded sample, showing a histogram of the peak-to-peak distances. (**o**) Overlay, using only a rigid registration, of a STORM image (magenta) of cultured BS-C-1 cells stained with antitubulin pre-expansion with a confocal image (green) of the same sample postexpansion. (**p**) RMS length measurement error of biological measurements calculated using the distortion vector field method[9] using STORM microscopy pre-expansion followed by confocal imaging of iExM-processed samples (~20× expanded) (blue line, mean; shaded area, ±1 s.d.; *n* = 3 samples).

(**Fig. 2j**, inset). The nanoscale axial resolution of iExM enabled clear visualization of microtubules of BS-C-1 cells in 3D (**Supplementary Videos 1** and **2**).

We applied iExM to preserved mouse tissues—including brain, liver and lung—to determine whether iExM could resolve ~20-nm biological structures in intact tissues. As shown in the inset of **Figure 2k** (single z-plane image; see **Fig. 2l** for the entire cellular context), the sidewalls of microtubules in mouse brain slices were resolvable on a confocal microscope. The distance between the two peaks of the fitted Gaussians was similar to that obtained in the cultured cell case (**Fig. 2m**; population data in **Fig. 2n**). The sidewalls of microtubules in cells of mouse lung and liver tissue slices were also easily resolved on confocal microscopes (**Supplementary Fig. 7a**–**h**). In addition to the visualization of the sidewalls of microtubules in tissues, we found that individual components of microtubule bundles in the mouse cortex could be resolved after 18-fold expansion (**Supplementary Fig. 7i**–**l**).

In addition to resolution, the ability to tell finely spaced objects apart, another optical parameter of interest is distortion across more extended length scales. Accordingly, we quantified the distortion caused by iExM over various length scales that corresponded to feature sizes of interest in cell biology. To measure distortion over scales of several microns, we compared pre-expansion images taken on a super-resolution microscope to postexpansion images taken on a conventional diffraction-limited microscope[1,2,9]. We prepared samples with secondary antibodies labeled

with STORM dyes and simultaneously applied DNA-conjugated secondary antibodies so they could be processed for iExM and visualized postexpansion. We coregistered the pre-expansion STORM image and postexpansion confocal image via a rigid transformation (**Fig. 2o**), and then we calculated the deformation vector field between the two images[1,2,9]. Although the image qualities enabled by STORM and iExM were compromised in this specific experiment because of the special requirements involved in imaging the same sample for both methods (e.g., each label will occur at half the antibody labeling density of a typical experiment, since we are dual labeling), the root mean square (RMS) alignment error between iExM and STORM was nonetheless small, about 2.5% of measurement length (**Fig. 2p**) over scales of several microns, similar to the 1–4% range of alignment errors previously determined for ExM[1,2,9]. We estimated the distortion of iExM across length scales of tens to hundreds of nanometers by examining the variation of microtubule diameter along 400-nm distances down the long axis of the microtubule. The estimated distortion was found to be 9 nm for cells and 13 nm for tissues (see **Supplementary Note 6** for details).

Nanoscale imaging of synapses

We next explored the utility of iExM in the context of resolving proteins within synapses. To improve brightness of expanded specimens, we pursued signal amplification using either DNA or locked nucleic acid (LNA) probes to increase the number of fluorophores associated with a single gel-anchored oligo (see **Supplementary Fig. 8** for schematic; see also **Supplementary Note 7**). We first examined synapses of cultured mouse hippocampal neurons. We labeled synapses with sets of antibodies that indicate putative excitatory (**Fig. 3a–c**) or inhibitory (**Fig. 3d–f**) synapses—anti-Homer1, anti-Bassoon, and anti-Glutamate receptor 1 (GluR1) for the former; anti-Gephyrin, anti-Bassoon, and anti-Gamma-aminobutyric acid receptor Aα1/anti-Gamma-aminobutyric acid receptor Aα2 ($GABA_AR\alpha1/\alpha2$; labeled with the same oligonucleotide strand) for the latter. It was possible not only to resolve the presynaptic scaffolding protein Bassoon from the postsynaptic scaffolding proteins Homer1 and Gephyrin, but also to resolve proteins within a synaptic compartment—resolving the neurotransmitter receptors GluR1 and $GABA_AR\alpha1/\alpha2$ from their respective postsynaptic scaffolding proteins as well (**Fig. 3c**,**f**). We observed the geometric organization of proteins within synapses to see, for example, how GluR1 proteins sometimes formed ring structures around Homer1 proteins (**Fig. 3g**, dotted circle in the upper right inset) as has been previously reported using STORM[10]. The isotropic 3D nature of iExM expansion allowed us to resolve structures organized along the optical axis of the microscope; for example, we resolved ring structures of GluR1 when the synaptic cleft was parallel to the microscope's optical axis (**Fig. 3g**, dotted circle in the bottom).

We demonstrated the ability of iExM to resolve synaptic structures in the mouse brain. We immunostained a mouse brain slice with antibodies against Bassoon and Homer1, expanded the brain slice 16-fold with iExM, and then imaged putative synapses within four different brain regions (overview in **Fig. 3h**; iExM images taken on a confocal microscope in **Fig. 3i–o**; see **Supplementary Fig. 9** for additional images taken with epifluorescence microscopy). The average distances between Bassoon and Homer1 observed in two regions within primary somatosensory cortex (indicated with Roman numerals i and ii in **Fig. 3h** and highlighted in **Fig. 3i**,**j**) were similar to each other (**Fig. 3p**,**q**) and to Bassoon–Homer distances observed in the dorsal striatum (indicated with Roman numeral iii in **Fig. 3h** and highlighted in **Fig. 3k**; see **Fig. 3r** for the population data). However, a fourth region, the medial pallidum (indicated with Roman numeral iv in **Fig. 3h** and highlighted in **Fig. 3l–o**), exhibited distances between Bassoon and Homer1 that were 50% longer (**Fig. 3s**), suggestive of a different synaptic architecture; furthermore, although putative synapses were evenly distributed in cortex and striatum, synapses in the pallidum were arranged in regularly spaced patterns as if they were tiling a cylindrical target (**Fig. 3l–o**; **Supplementary Video 3**). We used iExM to explore other regional heterogeneities in localization of presynaptic and postsynaptic proteins (**Supplementary Fig. 10** and **Supplementary Video 4**). Thus, iExM may be useful for analyzing the varying nanoscale configurations of proteins across brain circuits and regions, because it can support large-volume imaging with nanoscale precision.

We applied Brainbow adeno-associated viruses (AAVs)[11], in which Cre-expressing neurons are virally transduced to express, in random combinations, subsets of four fluorescent proteins (TagBFP, mTFP, mCherry, and EYFP), each fused to a farnesylation tag for membrane targeting. When such mouse brain slices were immunostained with antibodies against Homer1, as well as against fluorescent proteins (mCherry for **Fig. 3t**; EYFP for **Fig. 3u**), we found that postsynaptic proteins and membrane outlines could be covisualized (**Fig. 3t**,**u**). At synaptic contacts (as indicated by Homer1 staining) we observed less membrane-bound fluorophore (e.g., arrows of **Fig. 3t**,**u**), perhaps because the density of proteins at the synaptic cleft prevents the inward diffusion of membrane-anchored fluorophores. Thus iExM may be useful for mapping out how proteins are arranged in small, even nanoscale, compartments of neurons.

Nanoscale imaging of 3D mouse brain circuitry

We prepared Brainbow-AAV-labeled mouse brain samples as above and performed iExM with locked nucleic acid hybridization-based signal amplification. Brainbow-AAV-labeled dendritic spines in the molecular layer of the mouse hippocampal dentate gyrus are hard to resolve without expansion (**Fig. 4a**). In such samples processed with ~4.5×-expansion-factor protein-retention expansion microscopy (proExM, in which antibodies, genetically encoded fluorophores, or other proteins within a specimen are anchored to the swellable gel and then expanded[2]), dendritic spines could be identified and sometimes even distinguished from one another, but their shapes were difficult to analyze (**Fig. 4b**). After iExM the number, size, position, and shapes of dendritic spines were easily visualized, as is shown in the maximum intensity projection in **Figure 4c** (see **Supplementary Video 5** for 3D visualization; note that as in **Fig. 3t**,**u**, membrane-anchored fluorophores are less dense or even absent at the tips of spines, consistent with membrane-anchored fluorophore exclusion by postsynaptic proteins as hypothesized above; see **Supplementary Fig. 11**). In particular, the hollow space within neurons (**Fig. 4d–f**) and spines was easily visualized when we used membrane-localized fluorescent proteins (**Fig. 4f**; for more examples, see **Supplementary Fig. 12** and **Supplementary Video 6**). With iExM, it is possible to visualize structures such as spines along neural processes that extend over large 3D volumes; for example, along branching dendrites (shown in **Fig. 4g**; four sections of **Fig. 4g**

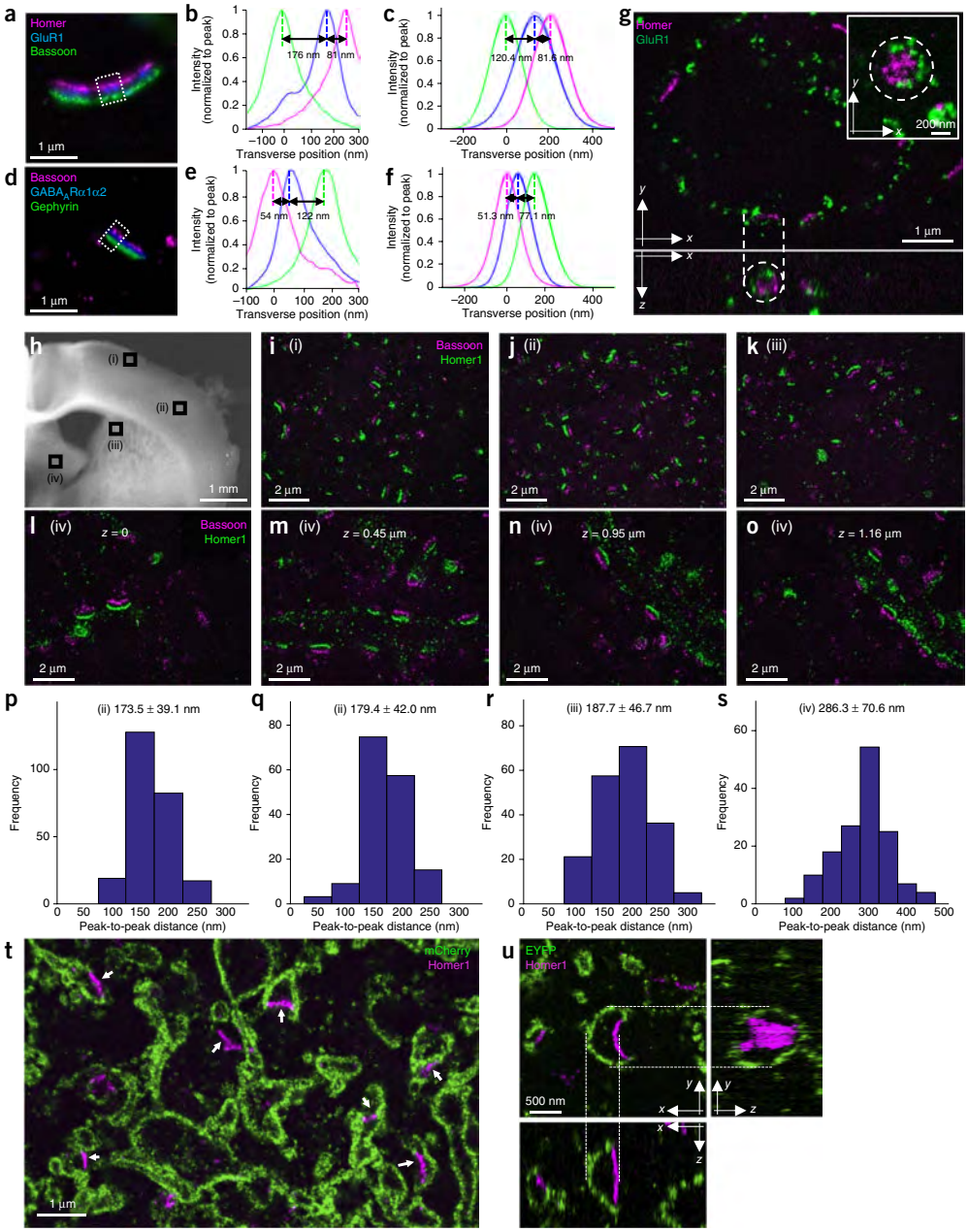

Figure 3 | Nanoscale-resolution imaging of synapses using iExM. (**a**) Epifluorescence image of cultured hippocampal neurons stained with antibodies against Homer1 (magenta), glutamate receptor 1 (GluR1, blue), and Bassoon (green), after ~13-fold expansion via iExM and DNA-hybridization-based signal amplification. Boxed regions are analyzed further in **b**. (**b**) Transverse profile of the three proteins imaged in the sample of **a** (in the boxed region) after normalizing to the peak (Homer1 in magenta, GluR1 in blue, Bassoon in green). (**c**) Sum of Gaussian functions fitted to curves as in **b** for ten synapses from one sample, normalized to peak (thick lines, mean; thin lines, ±1 s.d.). (**d**) As in **a**, but stained with antibodies against Bassoon (magenta), GABA$_A$Rα1/α2 (blue), and Gephyrin (green). (**e**) As in **b**, but for the boxed region in **d** (Bassoon in magenta, GABA$_A$Rα1/α2 in blue, Gephyrin in green). (**f**) As in **c**, but for the labels of **d**; 14 synapses from one sample. (**g**) Confocal z-stack (top, a single *xy*-plane; bottom, a single *xz*-plane; dotted lines connect corresponding points in the two cross-sections) of cultured hippocampal neurons with labeled Homer1 (magenta) and GluR1(green) after ~20-fold expansion via iExM. Inset of upper panel shows a zoomed-in image of a synapse (from another field of view) showing the circular distribution of GluR1 around Homer1. (**h**) Low-magnification widefield image of a mouse brain slice (corresponding to slide 57 of the Allen Brain Reference Atlas, P56 mouse, coronal sections) showing four regions, i–iv, that were imaged after expansion in **i**–**o** (i and ii, primary somatosensory cortex; iii, dorsal striatum; iv, medial pallidum). (**i**–**k**) Confocal images of three regions, i–iii, highlighted in **h** after labeling with anti-Bassoon (magenta) and anti-Homer1 (green) and 16-fold expansion via iExM. (**l**–**o**) Single *xy*-plane imaged at iv in **h** at different z-heights. (**p**–**s**) Population data of the Homer1–Bassoon separation (mean ± s.d.) measured in the four regions shown in **h**. The number of Homer1–Bassoon pairs analyzed was: **p**, 248 pairs from one specimen; **q**, 159 pairs from one specimen; **r**, 189 pairs from one specimen; **s**, 147 pairs from one specimen. (**t**,**u**) Confocal images of motor cortex areas (**t**, slide 57 of the Allen Brain Reference Atlas P56 mouse coronal sections; **u**, slide 47 of the same Atlas) after immunostaining and expansion. (**t**) Confocal image of the specimen after immunostaining with antibodies against Homer1 (magenta) and mCherry (green) and 16-fold expansion via iExM. (**u**) Z-stack confocal image of the specimen after immunostaining with antibodies against Homer1 (magenta) and EYFP (green) and 20-fold expansion via iExM. Upper left shows a single *xy*-plane image; right shows a single *yz*-plane image reconstructed from the z-stack image; bottom shows a single *xz*-plane image reconstructed from the z-stack image.

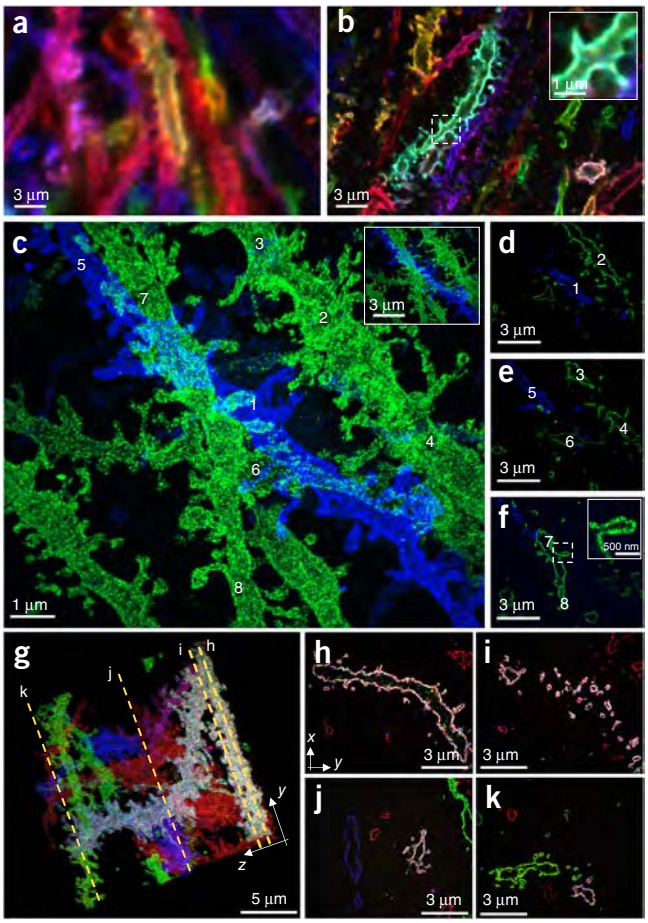

Figure 4 | Nanoscale-resolution imaging of mouse hippocampal brain circuitry. (**a**) Confocal image of immunostained Emx1-Cre mouse hippocampus with neurons expressing membrane-bound fluorescent proteins (Brainbow AAVs) before expansion. Blue, EYFP; red, TagBFP; green, mTFP. (**b**) As in **a**, but expanded 4.5-fold by the antibody-anchoring form of the ProExM protocol[2]. Blue, EYFP; red, TagBFP; green, mTFP. Inset shows a magnified image of a spine in the dotted box of **b**. (**c**–**f**) Confocal z-stack image of 20-fold-expanded mouse hippocampal circuitry with labeled EYFP (blue) and mCherry (green). (**c**) Maximum intensity projection of the stack shown in (**d**–**f**); numbers refer to neural processes that are highlighted within individual z-stacks in **d**–**f**. Inset shows a demagnified view of the image of **c** with the same scale bar as **a** and **b**. (**d**–**f**) Single *xy*-plane images at different z-heights from the bottom of the specimen. (**d**) z = 1.9 µm; (**e**) z = 2.4 µm; (**f**) z = 3.2 µm. See **Supplementary Video 5** for 3D video and surface rendering. Inset of **f** shows a magnified view of a spine in the dotted box of **f**. (**g**–**k**) Confocal z-stack image of 20-fold-expanded mouse hippocampal circuitry with labeled EYFP and mTFP (blue; both EYFP and mTFP were labeled in the same color), mCherry (green), and tagBFP (red). (**g**) Maximum intensity projection of the stack; dotted orange lines highlight four z-planes which yielded the images of **h**–**k**. (**h**–**k**) Single z-plane images of the stack of **g**. See **Supplementary Video 7** for 3D video.

are shown in **Fig. 4h**–**k**; see also **Supplementary Video 7**; further examples in **Supplementary Fig. 13** and **Supplementary Videos 8** and **9**). To some extent, neuronal geometries could even be resolved with epifluorescence microscopy (mouse cortex, 16-fold expansion via hp-iExM; **Supplementary Fig. 14**). Thus, iExM can be used to explore neural connectivity in 3D with spatial precision sufficient for resolving individual synaptic connections.

Can iExM be applied beyond two rounds? In principle we could perform the second round of expansion so that a third round would be possible by using a crosslinker whose cleaving chemistry is orthogonal to that of the first crosslinker. We found that it was possible to magnify a sample by 4.6 × 3.2 × 3.6 ~53-fold (see **Supplementary Note 8** for details; see **Supplementary Fig. 15** for 53-fold-expanded BS-C-1 cells after antibody-labeling tubulin). Although this might seem to imply an effective resolution of 300 nm / 53 = 5.7 nm, the actual resolution is limited by the size of antibodies, the use of DNA anchors (additional ~4.6-nm positional errors, as estimated above), and the broadening of the PSF by the gelation and expansion process (additional ~6 nm errors, as estimated above). However, with nanobody-based[12] or small-molecule tags[13] compatible with iExM, iterated expansion strategies may be able to further improve in resolution beyond 25 nm.

DISCUSSION

iExM achieves resolutions comparable to those of the highest performing forms of super-resolution light microscopy. Although expanded samples prepared with iExM can be quite large, they are transparent and homogeneous in refractive index (since they are 99.99% polymer and water and less than 0.01% original biomaterial), analogous to previous ExM versions[1–3,9], and thus may be amenable to fast, large-volume imaging modalities compatible with transparent tissues such as light-sheet microscopy[14]. Indeed, light-sheet imaging of ExM-processed tissues has recently been shown to be feasible[3]. With objective lenses of working distance ~8 mm available (for example, the Olympus 25× 0.9 NA[15]), ~400-µm-thick slices could be expanded by ~20× and imaged without further sectioning. iExM-processed samples are stiff enough to support postexpansion sectioning (e.g., with a vibratome); any sectioning error is effectively divided by the expansion factor in terms of impact on the biological information, and thus iExM could in principle help support the mapping of neural circuitry over large volumes, for example, entire neural circuits or even entire brains. The volumetric dilution of iExM results in a lower density of biomolecules and labels, but the additional room created by expansion can support amplification chemistries such as those used here or other variants of hybridization-based fluorescence amplification such as the hybridization chain reaction (HCR)[16]. In fact, we recently used HCR in the context of expanded brain tissues to visualize single RNAs within synaptic compartments of neurons in intact mouse brain circuits, taking advantage of the room made by expansion to append on the order of perhaps several dozen fluorophores to a single RNA strand[3].

iExM is a strategy, not a single chemistry, and thus could be applied to other fundamental ExM chemistries—for example, cleavable monomers that could support iterative removal of previous gels, as well as alternative polymer systems[17]. Since iExM concludes with nucleic acid strands (whose sequences code for protein identity) anchored throughout a polymer network at locations determined by the original protein locations, iExM may be able to support multiplexed *in situ* proteomics through serial hybridization of fluorescent strands as is done in DNA-PAINT[18]. We recently demonstrated serial hybridization readout of multiple RNAs using our ExFISH variant of ExM[3]. Because iExM decrowds protein labels to the point where signals become discontinuous as individual labels are separated, coded hybridization strategies where the same strand is imaged many times with different sets of probes may allow an exponential

number of proteins to be probed given a linear number of hybridization rounds—as has been previously done with RNA[19,20]. The additional room around biomolecules created by expansion could enable potentially complex reactions, including sequencing[21], to be conducted on expanded tissues, furthering the ability to read out the molecular composition of complex biological systems in a multiplexed, yet scalable, way. Finally, direct-anchoring versions of iExM may be possible, in which proteins or other biomolecules are directly anchored to the swellable polymer and then moved away from each other through repeated physical expansion. To achieve this, it would be important to develop ways to transfer the anchored biomolecules from the first swellable gel to the second. For example, in protein retention expansion microscopy (proExM), proteins (potentially including antibodies or fluorescent proteins) are directly anchored to the polymer gel and then expanded away from each other[2,9,22]; to create an iterative form of proExM, one would need novel chemical linkers that can support the covalent transfer of the proteins from the first gel to the second.

METHODS

Methods, including statements of data availability and any associated accession codes and references, are available in the online version of the paper.

Note: Any Supplementary Information and Source Data files are available in the online version of the paper.

ACKNOWLEDGMENTS

E.S.B. was funded by the HHMI-Simons Faculty Scholars Program; the NIH Director's Pioneer Award 1DP1NS087724; the New York Stem Cell Foundation-Robertson Award; the US Army Research Laboratory and the US Army Research Office under contract/grant number W911NF1510548; US-Israel Binational Science Foundation Grant 2014509; the Picower Institute Innovation Fund; IARPA D16PC00008; NIH grants 1R01MH110932, 1R43MH101943, 1R01MH103910, 1R01EY023173, and 2R01DA029639; the IET A.F. Harvey Prize; the Open Philanthropy Project; the Halis Family Foundation; and the MIT Media Lab. J.-B.C. was supported by the Simons Postdoctoral Fellowship. F.C. was supported by the NSF Fellowship and Poitras Fellowship. Y.-G.Y., J.S.K., and H.-J.S. were supported by Samsung Scholarships. P.W.T. and A.T.W. were supported by Hertz Foundation fellowships. Confocal imaging was performed in the W.M. Keck Facility for Biological Imaging at the Whitehead Institute for Biomedical Research J.-B.C. was supported by the Center for Neuroscience Imaging Research. D.C. was funded by NIH grants R21GM114852 and R01MH110932. We acknowledge W. Salmon (MIT) for her assistance with confocal imaging. STORM imaging shown in **Figure 2o** was performed in the Center for Brain Science at Harvard University. We acknowledge E. Garner, C. Wivagg, and S. Turney (Harvard) for allowing us to use the N-STORM microscope and their assistance with STORM imaging. We acknowledge D. Park (MIT) for assistance with the preparation of cultured neurons. We also acknowledge S. Shim, Y. Sigal, C. Speer, M. Thanawala, D. Kim, M. Sauer, and S. Alon for helpful discussions. We acknowledge University of Michigan, Ann Arbor for providing antibodies against Brainbow fluorescent proteins.

AUTHOR CONTRIBUTIONS

E.S.B. and J.-B.C. conceived the main idea and designed experiments. P.W.T. conceived hp-iExM strategy. J.-B.C. performed immunostaining and expanded specimens. J.-B.C., F.C., and A.W. developed re-embedding process. J.-B.C. calculated RMS error of iExM. F.C. conceived signal amplification methods. E.E.J. performed immunostaining. Y.-G.Y. performed deconvolution and denoising and developed the iExM simulator. H.-J.S. and N.P. performed the brainbow virus injection and perfusion. Y.-G.Y. and S.A. created 3D videos. H.B. contributed STORM data in **Figure 2a–c**. J.-B.C. performed STORM imaging for **Figure 2o,p**. D.C. provided antibodies against Brainbow fluorescent proteins. J.-B.C. and J.S.K. imaged samples and performed image processing. J.-B.C. performed statistical analysis. E.S.B. and J.-B.C. wrote the paper. All authors contributed to editing of the paper. E.S.B. supervised this work.

COMPETING FINANCIAL INTERESTS

The authors declare competing financial interests: details are available in the online version of the paper.

1. Chen, F., Tillberg, P.W. & Boyden, E.S. Expansion microscopy. *Science* **347**, 543–548 (2015).
2. Tillberg, P.W. *et al.* Protein-retention expansion microscopy of cells and tissues labeled using standard fluorescent proteins and antibodies. *Nat. Biotechnol.* **34**, 987–992 (2016).
3. Chen, F. *et al.* Nanoscale imaging of RNA with expansion microscopy. *Nat. Methods* **13**, 679–684 (2016).
4. O'Connell, P.B.H. & Brady, C.J. Polyacrylamide gels with modified cross-linkages. *Anal. Biochem.* **76**, 63–73 (1976).
5. Kurenkov, V.F., Hartan, H.-G. & Lobanov, F.I. Alkaline hydrolysis of polyacrylamide. *Russ. J. Appl. Chem.* **74**, 543–554 (2001).
6. Weber, K., Rathke, P.C. & Osborn, M. Cytoplasmic microtubular images in glutaraldehyde-fixed tissue culture cells by electron microscopy and by immunofluorescence microscopy. *Proc. Natl. Acad. Sci. USA* **75**, 1820–1824 (1978).
7. Dempsey, G.T., Vaughan, J.C., Chen, K.H., Bates, M. & Zhuang, X. Evaluation of fluorophores for optimal performance in localization-based super-resolution imaging. *Nat. Methods* **8**, 1027–1036 (2011).
8. Aquino, D. *et al.* Two-color nanoscopy of three-dimensional volumes by 4Pi detection of stochastically switched fluorophores. *Nat. Methods* **8**, 353–359 (2011).
9. Chozinski, T.J. *et al.* Expansion microscopy with conventional antibodies and fluorescent proteins. *Nat. Methods* **13**, 485–488 (2016).
10. Dani, A., Huang, B., Bergan, J., Dulac, C. & Zhuang, X. Superresolution imaging of chemical synapses in the brain. *Neuron* **68**, 843–856 (2010).
11. Cai, D., Cohen, K.B., Luo, T., Lichtman, J.W. & Sanes, J.R. Improved tools for the Brainbow toolbox. *Nat. Methods* **10**, 540–547 (2013).
12. Olivier, N., Keller, D., Gönczy, P. & Manley, S. Resolution doubling in 3D-STORM imaging through improved buffers. *PLoS One* **8**, e69004 (2013).
13. Wombacher, R. & Cornish, V.W. Chemical tags: applications in live cell fluorescence imaging. *J. Biophotonics* **4**, 391–402 (2011).
14. Chen, B.-C. *et al.* Lattice light-sheet microscopy: imaging molecules to embryos at high spatiotemporal resolution. *Science* **346**, 1257998 (2014).
15. Ke, M.-T., Fujimoto, S. & Imai, T. SeeDB: a simple and morphology-preserving optical clearing agent for neuronal circuit reconstruction. *Nat. Neurosci.* **16**, 1154–1161 (2013).
16. Choi, H.M.T. *et al.* Programmable *in situ* amplification for multiplexed imaging of mRNA expression. *Nat. Biotechnol.* **28**, 1208–1212 (2010).
17. Cipriano, B.H. *et al.* Superabsorbent hydrogels that are robust and highly stretchable. *Macromolecules* **47**, 4445–4452 (2014).
18. Jungmann, R. *et al.* Multiplexed 3D cellular super-resolution imaging with DNA-PAINT and Exchange-PAINT. *Nat. Methods* **11**, 313–318 (2014).
19. Lubeck, E., Coskun, A.F., Zhiyentayev, T., Ahmad, M. & Cai, L. Single-cell *in situ* RNA profiling by sequential hybridization. *Nat. Methods* **11**, 360–361 (2014).
20. Chen, K.H., Boettiger, A.N., Moffitt, J.R., Wang, S. & Zhuang, X. RNA imaging. Spatially resolved, highly multiplexed RNA profiling in single cells. *Science* **348**, aaa6090 (2015).
21. Lee, J.H. *et al.* Highly multiplexed subcellular RNA sequencing. *in situ*. *Science* **343**, 1360–1363 (2014).
22. Ku, T. *et al.* Multiplexed and scalable super-resolution imaging of three-dimensional protein localization in size-adjustable tissues. *Nat. Biotechnol.* **34**, 973–981 (2016).

ONLINE METHODS

A step-by-step protocol of this method can be found in the **Supplementary Protocol**. A table of all chemicals can be found in **Supplementary Table 1**.

DNA, locked nucleic acids, and primary and secondary antibody preparation. Oligonucleotides were purchased from Integrated DNA technologies (IDT) with standard desalting purification (see **Supplementary Tables 2–8** for the sequences). Locked nucleic acids (LNAs) were purchased from Exiqon with high-performance liquid chromatography (HPLC) purification (see **Supplementary Table 9** for the sequences). Primary and secondary antibodies were purchased from multiple vendors (see **Supplementary Tables 10–12**). Primary antibodies used were rabbit anti-beta tubulin (Abcam ab6046, 1:100), rabbit anti-Homer1 (Synaptic systems 160003, 1:200), guinea pig anti-Homer1 (Synaptic systems 160004, 1:200), mouse anti-Homer1 (Synaptic systems 160011, 1:200), mouse anti-Bassoon (Enzo ADI-VAM-PS003-F, 1:200), guinea pig anti-Bassoon (Synaptic systems 141004, 1:200), mouse anti-Gephyrin (Synaptic systems 147011, 1:200), rabbit anti-$GABA_AR\alpha1$ (Synaptic systems 224203, 1:200), rabbit anti-$GABA_AR\alpha2$ (Synaptic systems 224103, 1:200), rabbit anti-GluR1 (Abcam ab31232, 1:100), guinea pig anti-TagRFP (Kerafast EMU107, 1:200), rabbit anti-mCherry (Abcam ab167453, 1:200), rat anti-mCherry (ThermoFisher M11217, 1:200), rat anti-mTFP (Kerafast EMU103, 1:200), and chicken anti-GFP (Kerafast EMU101, 1:400). Secondary antibodies used were goat anti-chicken (ThermoFisher A-11039, 10 μg/μL), goat anti-rat (ThermoFisher A-11081, 10 μg/μL), goat anti-guinea pig (Biotium CF633 conjugated, 10 μg/μL), and donkey anti-rabbit (ThermoFisher A31573, 1:100). Secondary antibodies from Jackson ImmunoResearch were used to make DNA-conjugated secondary antibodies, using the following reagents: donkey anti-rabbit (711-005-152), donkey anti-chicken (703-005-155), donkey anti-rat (712-005-153), donkey anti-guinea pig (706-005-148), and donkey anti-mouse (715-005-151). For DNA-conjugated secondary antibodies, 10 μg/μL was used for cultured cell lines/neurons, and 20 μg/μL was used for tissue slices. Oligonucleotides with a 5′ amine modification (see **Supplementary Table 2** for the sequences) were conjugated to secondary antibodies using a modified protocol from a commercial kit (Solulink, Antibody-Oligonucleotide All-in-One conjugation kit; please visit http://expansionmicroscopy.org/ to find step-by-step instructions for the DNA–antibody conjugation).

Cultured BS-C-1 cell preparation. BS-C-1 cells (American Type Culture Collection, product number CCL-26) were cultured in Nunc Lab-Tek II chambered coverglasses (ThermoFisher, 155409) with Eagle's Minimum Essential Medium supplemented with 10% heat-inactivated fetal bovine serum (FBS) and 1% penicillin–streptomycin, and the cells were incubated at 37 °C in 5% CO_2.

Cultured hippocampal neuron preparation. Hippocampal neurons were prepared from postnatal day 0 or day 1 Swiss Webster (Taconic) mice as previously described[23,24], but with the following modifications. Hippocampal tissues were isolated and digested with 50 units of papain for 6–8 min, and then the digestion was stopped with ovomucoid trypsin inhibitor. 10,000–20,000 cells were plated in Matrigel (BD Biosciences)-coated 96-well glass-bottom plates with 100 μL of plating medium containing MEM (Life Technologies), glucose (33 mM, Sigma), transferrin (0.01%, Sigma), Hepes (10 mM), Glutagro (2 mM, Corning), insulin (0.13%, Millipore), B27 supplement (2%, Gibco), and heat-inactivated FBS (7.5%, Corning). AraC (0.002 mM, Sigma) was added when glial density reached 50–70% of confluence. Neurons were cultured at 37 °C in humidified 5% CO_2.

Brainbow AAV injection and brain preparation. All the following procedures involving animals were approved by the Massachusetts Institute of Technology Committee on Animal Care and were in accordance with the National Institutes of Health Guide for the Care and Use of Laboratory Animals. 4 Emx1-Cre mice ages ~3–5 months old were used. Mice were used without regard for sex. Brainbow rAAV (AAV9.hEF1a.lox.TagBFP.lox.eYFP.lox.WPRE.hGH-InvBYF and AAV9.hEF1a.lox.mCherry.lox.mTFP1.lox.WPRE.hGH-InvCheTF; University of Pennsylvania, Penn Vector Core) was injected into Emx1-Cre mice[11]. Adult Emx1-Cre mice were first head fixed to a stereotaxic apparatus, and a small (~0.5 mm^2) craniotomy was performed under continuous isoflurane anesthesia. A 34-gauge injection needle preloaded with the AAV solution (7.5×10^{12} genome copy/mL) was then inserted into the brain to a depth of ~500 μm from the cortical surface, and the virus was infused at a rate of 0.2 μL/min. After injecting 2 μL of the virus solution, the needle was left at the injection site for an additional 5 min to allow for viral diffusion. Mice were allowed to recover from surgery and express virus for 3–4 weeks before transcardial perfusion. Using isoflurane, mice were deeply anesthetized and perfused with 30 mL room temperature 1× PBS, and then 30 mL room-temperature fixative solution (4% paraformaldehyde in 1× PBS). Brains were then harvested and stored in the same fixative at 4 °C for 24 h. 100-μm- or 150-μm thick brain slices were prepared by slicing brains with 100 mM glycine in 1× PBS on a vibratome (Leica VT1000s). The slices were stored in 1× PBS at 4 °C until staining.

Immunostaining of tissues (except the microtubule staining of mouse tissue slices). All following steps were conducted at room temperature with gentle shaking, unless otherwise noted. To stain Brainbow slices, two different conditions were used. To stain only Brainbow AAV fluorescent proteins (FPs), Brainbow mouse brain slices were first permeabilized and blocked in '0.5T' blocking buffer (0.5% Triton X-100, 5% normal donkey serum (NDS), 1× PBS) for 2 h. Slices were then incubated with primary antibodies (see **Supplementary Tables 10** and **11** for details) in '0.25T' blocking buffer (0.25% Triton X-100, 5% NDS, 1× PBS) for 2–3 d at 4 °C with gentle shaking. Slices were washed in 0.25T blocking buffer four times for 30 min each time. Slices were incubated with DNA-conjugated secondary antibodies in hybridization buffer (2× SSC buffer, 10% dextran sulfate, 1 mg/mL yeast tRNA, 5% NDS, 0.1% Triton X-100) overnight and washed in 0.25T blocking buffer four times for 30 min each time. Slices were then incubated with DNAs with a 5′ acrydite modification at a concentration of 1 ng/μL in hybridization buffer overnight, and then they were washed in 0.25T blocking buffer four times for 30 min each time.

To stain synaptic proteins, or synaptic proteins and Brainbow FPs, Brainbow slices were first permeabilized and blocked in '0.1T' blocking buffer (0.1% Triton X-100, 1× PBS, 5% NDS) for 2 h. Primary antibody staining and subsequent washing steps

doi:10.1038/nmeth.4261

were identical to those of the FP staining protocol described above, but they were conducted in 0.1T blocking buffer. DNA-conjugated antibody and DNA-staining steps were identical to those of the FP staining protocol. Subsequent washing steps were conducted in 0.1T blocking buffer. To stain FPs for proExM the permeabilization, primary antibody staining, washing steps, and secondary antibody staining were conducted in 0.1T blocking buffer.

Immunostaining of tubulin in cultured cells and tissue slices. All of the following steps were conducted at room temperature, unless otherwise noted. Cells were first washed in 1× PBS three times; then they were extracted in cytoskeleton extraction buffer[25] (0.2% Triton X-100, 0.1 M 1,4-piperazinediethanesulfonic acid (PIPES), 1 mM ethylene glycol-bis(2-aminoethylether)-N,N,N′,N′-tetraacetic acid (EGTA), 1 mM magnesium chloride, pH 7.0) for 1 min and then fixed in tubulin fixation solution (3% formaldehyde, 0.1% glutaraldehyde, 1× PBS) for 10 min, followed by reduction with 0.1% sodium borohydride in 1× PBS for 7 min and washing with 100 mM glycine in 1× PBS three times for 5 min each time. Cells were permeabilized and blocked in 0.2T blocking buffer (0.2% Triton X-100, 1× PBS, 5% NDS) for 10 min and incubated with rabbit anti-beta tubulin antibody in '0.2T' blocking buffer at a concentration of 10 μg/mL for 1 h, and then they were washed in 1× PBS three times. Cells were incubated with DNA-conjugated anti-rabbit secondary antibody (RbA1′ in **Supplementary Table 12**) in hybridization buffer at a concentration of 10 μg/mL for 1 h with gentle shaking, then they were washed in 1× PBS three times. Cells were incubated with DNA (A1 5′ acrydite 3′ Alexa 488 in **Supplementary Table 3**) in hybridization buffer at a concentration of 0.5 ng/μL for 1 h with gentle shaking, then they were washed three times in 1× PBS.

To stain microtubules of mouse tissue slices, Thy1–YFP mice were deeply anesthetized using isoflurane and perfused with 30 mL room temperature 1× PBS. Brains, livers, and lungs were then harvested and sliced on a vibratome (Leica VT1000s) to a thickness of 100 μm in 1× PBS. Slices were extracted in cytoskeleton extraction buffer[25] for 5 min with gentle shaking, and then they were fixed in tubulin fixation solution for 30 min with gentle shaking, followed by reduction with 0.1% sodium borohydride in 1× PBS for 7 min with gentle shaking and washing with 100 mM glycine in 1× PBS three times with gentle shaking for 10 min each time.

Slices were permeabilized and blocked in 0.2T blocking buffer (0.2% Triton X-100, 5% NDS, 1× PBS) for 2 h with gentle shaking. Primary antibody staining and all washing steps were identical to those of the the synaptic protein staining protocol, but they were conducted in 0.2T blocking buffer. DNA-conjugated antibody and DNA staining steps were identical to those of the synaptic protein staining protocol.

Immunostaining of synaptic proteins in cultured neurons. All following steps were conducted at room temperature, unless otherwise noted. Cultured neurons were fixed 2 weeks after initial plating. Cultured neurons were first washed in 1× PBS three times, and then they were fixed with 4% formaldehyde in 1× PBS for 10 min and washed with 100 mM glycine in 1× PBS three times for 5 min each time. Subsequent procedures were identical to the microtubule staining of cultured cells.

First-round expansion except for triple-round expansion experiments. After immunostaining, cultured cells, neurons, and tissue slices were first incubated in pregel incubation solution (see **Supplementary Table 13** for details) overnight at 4 °C. After the incubation, specimens were incubated in 1st gelation solution (**Supplementary Table 13**) twice for 30 min each time at 4 °C. For cultured cells and neurons, 200 μL of 1st gelation solution was added to each well and then incubated at 37 °C for 3 h. For tissue slices, slices were placed between two pieces of no. 1 coverglass separated by another no. 1 coverglass, and then they were incubated at 37 °C for 3 h.

After the incubation, gels (including cultured cells, neurons, and tissue slices) were incubated with Proteinase K at a concentration of 8 units/mL (1:100 dilution) in digestion buffer (50 mM Tris pH 8, 1 mM EDTA, 0.5% Triton-X100, 0.8 M guanidine HCl) overnight at room temperature with gentle shaking. Digested gels were next placed in an excess volume of fresh distilled (DI) water for three periods (2 h, 2 h, overnight) at room temperature with gentle shaking.

Re-embedding and DNA hybridization except for triple-round expansion experiments. All of the following steps were conducted at room temperature with gentle shaking, unless otherwise noted. Expanded gels were incubated in a freshly prepared re-embedding solution (**Supplementary Table 13**) twice for 30 min each time. After the incubation, gels were placed between two pieces of no. 1 coverglass and then incubated at 37 °C for 1.5 h in a nitrogen-filled chamber. Following the incubation, gels were detached from the coverglass and then washed in DNA hybridization buffer (20% (v/v) formamide in 4× saline-sodium citrate (SSC) buffer) for 30 min to remove any unreacted monomers from gels.

Gels that would not undergo signal amplification were incubated with DNAs (see **Supplementary Tables 4** and **10** for details) at a concentration of 0.5 ng/μL in DNA hybridization buffer overnight, and then they were washed in DNA hybridization buffer three times, for 2 h, 2 h, and overnight.

Gels that would undergo DNA- or LNA-hybridization-based signal amplification were incubated with linker DNAs (see **Supplementary Tables 4** and **10** for details) at a concentration of 2 ng/μL in DNA hybridization buffer overnight, and then they were washed in DNA hybridization buffer three times, for 2 h, 2 h, and overnight.

Second-round expansion except for triple-round expansion experiments. All of the following steps were conducted at room temperature with gentle shaking, unless otherwise noted. For hp-iExM, gels were incubated in a freshly prepared hp-iExM 2nd gel solution (**Supplementary Table 13**) twice for 30 min each. After this incubation, gels were placed between two pieces of no. 1 coverglass and then incubated in a nitrogen-filled chamber at 37 °C for 1.5 h. After this incubation, gels were incubated in 0.2 M NaOH overnight and washed in DI water multiple times until the size of the gels plateaued.

For iExM, gels were incubated in a freshly prepared iExM 2nd gel solution (**Supplementary Table 13**) twice for 30 min minutes each. After this incubation, gels were placed between two pieces of no. 1 coverglass, and then they were incubated in a nitrogen-filled chamber at 37 °C for 1.5 h. After this incubation, gels were

incubated in 0.2 M NaOH for 1 h. Gels were washed in DNA hybridization buffer twice for 30 min each time, and then they were incubated with fluorophore-tagged DNAs for DNA-hybridization-based signal amplification and fluorophore-tagged LNAs for LNA-hybridization-based signal amplification at a concentration of 0.5 ng/μL in DNA hybridization buffer overnight, and then they were washed in DNA hybridization buffer three times (2 h, 2 h, and overnight). Gels were then washed in 0.2× PBS multiple times for DNA-hybridization-based signal amplification and in DI water for LNA-hybridization-based signal amplification until the size of the gels plateaued.

Protein retention expansion microscopy. Immunostained brain slices were first incubated in 6-((acryloyl)amino)hexanoic acid, succinimidyl ester (AcX; resuspended in anhydrous DMSO at a concentration of 10 mg/mL and then diluted in 1× PBS at a concentration of 0.1 mg/mL) at room temperature overnight with gentle shaking. Slices were then incubated in monomer solution (1× PBS, 2 M NaCl, 8.625% (w/w) sodium acrylate, 2.5% (w/w) acrylamide, 0.15% (w/w) N,N′-methylenebisacrylamide (BIS), 0.2% (w/w) ammonium persulfate (APS), 0.2% (v/v) tetramethylethylenediamine (TEMED), 0.01% (w/w) 4-hydroxy-2,2,6,6-tetramethylpiperidin-1-oxyl (H-TEMPO)) twice for 30 min each time at 4 °C and placed between two pieces of no. 1 coverglass separated by another no. 1 coverglass and then incubated in a humidified 37 °C incubator for 2 h. Following the incubation, gels were digested in Proteinase K at a concentration of 8 units/mL in 50 mM Tris (pH 8) with 1 mM EDTA, 0.5% Triton X-100, and 1 M NaCl overnight at room temperature with gentle shaking and then expanded in DI water several times until the size of gels plateaued.

Imaging. Imaging was performed on an Andor spinning disk confocal microscope with a 40× 1.15 NA water-immersion objective (**Fig. 2d**,**g**,**k**,**l**,**o**; **Fig. 3g**,**i–o**,**t**,**u**; **Fig. 4**; **Supplementary Figs. 1b**,**2b**,**7**, and **10–13**) or Nikon Eclipse Ti inverted microscope with the same objective (**Fig. 3a**,**d**,**h**; **Supplementary Figs. 1a**,**9**,**14**, and **15**). Background of images was corrected by using the 'subtract background' function implemented in Fiji with a 50-pixel-wide 'rolling ball' algorithm.

Expansion factor measurement. To determine the expansion factors for each round of expansion, we imaged whole specimens (tissues and cultured cells) with a widefield microscope before versus after the expansion of the first gel. The expansion factor for the first round was then determined by measuring the distance between two landmarks in the specimen before versus after the first round of expansion. The expansion factor of the second round was determined in the same way.

Root mean square error measurement. RMS error measurement was performed in a similar way to that of previous studies[1,9]. Briefly, STORM images before expansion and confocal images after expansion were registered using rigid body registration as implemented in Fiji (Plugins → Registration → TurboReg → Rigid Body/Accurate/Manual)[1]. After the registration, deformation vector fields were calculated by using Elastix and Transformix as in ref. 9 (see Supplementary Protocol 1 of ref. 9 for details).

Deconvolution and denoising. Images shown in **Figure 2g** were deconvolved using custom-written MATLAB code that uses the Richardson–Lucy algorithm with wavelet regularization and a theoretical point-spread function. The deconvolution was performed with a GPU (NVidia, Tesla K40c). For **Figure 4c–k**, **Supplementary Figures 10–13**, and **Supplementary Videos 5–9**, the images were first deconvolved, and then the background and signals from nonspecifically bound fluorophores were removed by using connected component analysis[26].

Stochastic optical reconstruction microscopy imaging. BS-C-1 cells were cultured, extracted, fixed, and stained with a primary antibody as in "Immunostaining of tubulin in cultured cells and tissue slices." For **Figure 2a–c**, primary-antibody-stained cells were incubated with Alexa 647 conjugated anti-rabbit antibody (ThermoFisher A-31573, 20 μg/μL) in 0.2T blocking buffer for 30 min, and they werewashed in 1× PBS three times. STORM imaging was performed in STORM imaging buffer (100 mM Tris, pH 8.0, 50 mM NaCl, 1% β-Mercaptoethanol, 5% glucose, 1 μg/μL glucose oxidase, 40 μg/mL catalase) on a custom-built STORM microscope using the oblique-incidence geometry. For **Figure 2o**, primary-antibody-stained cells were incubated with a mixture of Alexa-647-conjugated anti-rabbit secondary antibody (13.3 μg/mL) and DNA-conjugated anti-rabbit secondary antibody (13.3 μg/mL, RbA1′) in hybridization buffer for 1 h at room temperature with gentle shaking and then washed in 1× PBS three times. After the washes, STORM imaging was performed on a commercial Nikon N-STORM microscope in total internal reflection fluorescence (TIRF) mode in STORM imaging buffer (1 M Tris, pH 8.0, 50 mM NaCl, 1% β-Mercaptoethanol, 5% glucose, 1 μg/μL glucose oxidase, 40 μg/mL catalase). After STORM imaging, cells were washed in 1× PBS and then incubated with DNA (A1 5′ acrydite 3′ Alexa 488 in **Supplementary Table 3**) in hybridization buffer at a concentration of 0.5 ng/μL for 1 h at room temperature with gentle shaking then washed three times in 1× PBS.

Statistics. In this study, the sample sizes were decided not based upon a power analysis, since the goal was to develop a new technology. As noted in ref. 27, "in experiments based on the success or failure of a desired goal, the number of animals required is difficult to estimate." As was also noted in this paper, "the number of animals required is usually estimated by experience instead of by any formal statistical calculation, although the procedures will be terminated [when the goal is achieved]."[27] The sample sizes of this study reflect our past experience in developing ExM technologies[1–3]. For animal studies, sample-size estimation was not performed. Exclusion, randomization, and blinding of samples were not performed.

Triple-round expansion. All following steps were conducted at room temperature with gentle shaking, unless otherwise noted. Immunostaining of BS-C-1 cells, pregel incubation, first-gel synthesis, re-embedding, and second-gel synthesis steps were identical to those of the iExM procedure for BS-C-1 cells with labeled tubulin, but with the following modifications. RbB1′ and DNA B1 5′ acrydite were used during the staining step. Pregel incubation solution, 1st gel solution, and 1st re-embedding solution shown in **Supplementary Table 14** were used to form a 1st

doi:10.1038/nmeth.4261

swellable gel and re-embedding gel. After the re-embedding, gels were incubated with DNA B1′ A2 5′ acrydite (**Supplementary Table 8**). 2nd gel solution shown in **Supplementary Table 14** was used to form a 2nd swellable gel.

After the 2nd gel formation, gels were incubated in 0.25 M tris (2-carboxyethyl)phosphine (TCEP; 1 M stock solution of TCEP diluted in 1 M Tris–HCl pH 8.0) overnight and then expanded in DI water three times. Expanded gels were re-embedded again in 2nd re-embedding solution (**Supplementary Table 14**), incubated with a linker DNA (A2′ 4LNA-A1′ 5′ acrydite) in DNA hybridization buffer overnight at a concentration of 2 ng/μL, and then washed in DNA hybridization buffer three times for 2 h, 2 h, and overnight.

Gels were then embedded in 3rd gel solution (**Supplementary Table 14**) and digested in 0.2 M NaOH for 1 h. Gels were then washed in DNA hybridization buffer and incubated with fluorophore-tagged LNA (LNA-A1 3′atto 565) at a concentration of 0.5 ng/μL in DNA hybridization buffer overnight, and then they were washed in DNA hybridization buffer three times for 2 h, 2 h, and overnight. Gels were then washed in DI water multiple times.

MATLAB simulation of iterative expansion microscopy images. We developed a simulator of iExM images of microtubules labeled with DNA-conjugated secondary antibodies (code contained in **Supplementary Software** and described in **Supplementary Fig. 2**). Simulation of iExM was performed by first creating a cylinder with an inner radius of R_i and outer radius of R_o. 5′ acrydite moieties were randomly assigned to voxels within the cylindrical volume to simulate the stochastic staining of a microtubule. To gauge the impact of the broadening of the PSF on the simulation (**Supplementary Fig. 6c**), the positions of the 5′ acrydite moieties were randomly perturbed with an s.d. E_p (parameter 'PositionE' in the MATLAB code). Then, the cylindrical volume was projected onto a 3D image stack by convolving the volume with the 3D point-spread-function (PSF) of a confocal microscope with an objective lens of 40× magnification and 1.15 NA. Then the volume was down sampled by pixel binning in the lateral dimension (with a pixel size of 6 nm) and subsampled in the axial dimension to incorporate the pixel pitch and the z-step size of the microscope. The simulation was performed multiple times with varying R_i and R_o.

Once the microtubule profiles with various combinations of R_i and R_o were generated, we fitted the simulated profiles with a sum of two Gaussians, and the peak-to-peak distances of the fitted sum of two Gaussians were measured. The measured peak-to-peak distances were compared with the peak-to-peak distances of each experimental microtubule profile. If the difference between these two distances was smaller than a single pixel size of the simulation (6 nm), then the R_i and R_o values of the corresponding simulated profile were retained for further analysis. The collected R_i and R_o values were averaged to find an average inner and outer radius of the DNA layer best fitted to experimental microtubule profiles. For example, the average R_i and R_o were 30.6 nm and 34.8 nm, respectively, for the experimental microtubule profile shown in **Supplementary Figure 2c**.

Code availability. iExM image simulator is contained in **Supplementary Software**.

Data availability statement. The data that support the findings of this study are available from the corresponding author upon request. Source data for **Figures 1** and **2** are available online

23. Klapoetke, N.C. *et al.* Independent optical excitation of distinct neural populations. *Nat. Methods* **11**, 338–346 (2014).
24. Chow, B.Y. *et al.* High-performance genetically targetable optical neural silencing by light-driven proton pumps. *Nature* **463**, 98–102 (2010).
25. Vaughan, J.C., Dempsey, G.T., Sun, E. & Zhuang, X. Phosphine quenching of cyanine dyes as a versatile tool for fluorescence microscopy. *J. Am. Chem. Soc.***135**, 1197–1200 (2013).
26. Legant, W.R. *et al.* High-density three-dimensional localization microscopy across large volumes. *Nat. Methods* **13**, 359–365 (2016).
27. Dell, R.B., Holleran, S. & Ramakrishnan, R. Sample size determination. *ILAR J.***43**, 207–213 (2002).

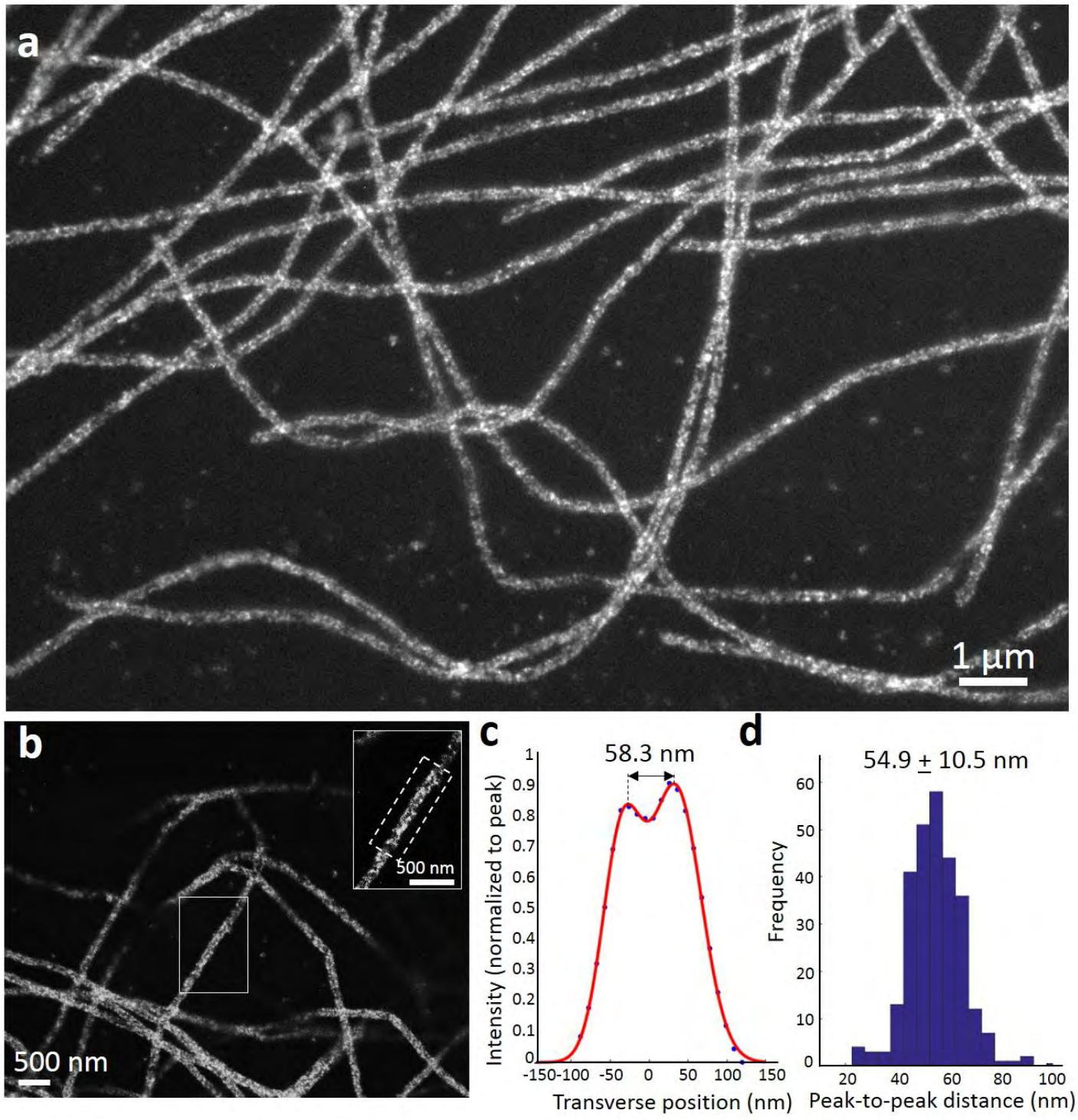

Supplementary Figure 1

hp-iExM processed microtubules.

(**a**) Epifluorescence image of cultured BS-C-1 cells immunostained with an antibody against beta tubulin, and expanded ~16-fold via hp-iExM. (**b**) Confocal image of BS-C-1 cells with labeled microtubules, after ~16-fold

expansion via hp-iExM. The inset in upper right zooms in on the small box at center. (**c**) Transverse profile of microtubules in the boxed region (dotted lines) of the inset of **b** after averaging down the long axis of the box and then normalizing to the peak (blue dots), with superimposed fit with a sum of two Gaussians (red lines). The peak-to-peak distance of the two Gaussian functions was 58.3 nm. (**d**) Population data for 277 microtubule segments from three expanded samples, showing a histogram of the peak-to-peak distances (calculated as in **c**).

Nature Methods: doi:10.1038/nmeth.4261

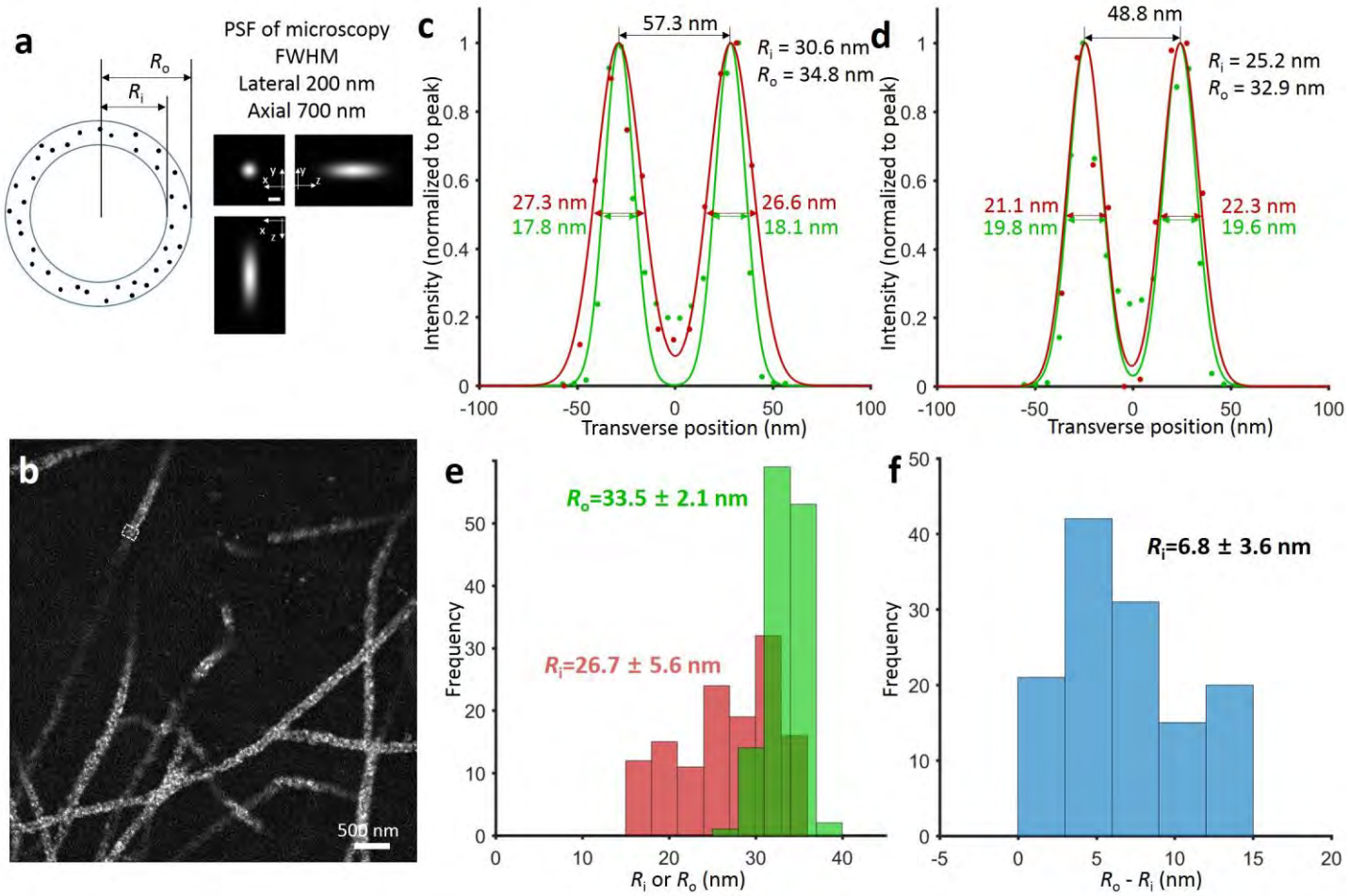

Supplementary Figure 2

Simulation of iExM imaging of microtubules.

(**a**) Schematic of simulation strategy (see **Supplementary Note 2** for details), along with depiction of the calculated point-spread function of the microscope we used (a spinning disk confocal microscope with a pinhole size of 50 µm equipped with a 40x NA1.15 objective lens). Scale bar, 200 nm. (**b**) Confocal microscope image of microtubules from cultured BS-C-1 cells after 20-fold expansion via iExM. The microtubule segment in the boxed region was analyzed in **c**. (**c**) Transverse profile (red dots) of the microtubule segment in the boxed region of **b** with superimposed fit with a sum of two Gaussians (red line) and simulated (using the model of **Supplementary Fig. 2a**) microtubule profile with a R_i of 30.6 nm and R_o of 34.8 nm (green dots) with superimposed fit with a sum of two Gaussians (green line). See section 'MATLAB simulation of iExM images' of the Methods for details of the fitting. The green and red numbers indicate the full width at half maximum for individual microtubule sidewalls, both simulated and real (see **Supplementary Fig. 6** for more analyses). (**d**) As in **c**, but for a different region (not shown in **b**). (**e**) Population data for 129 microtubule segments from one culture (numbers indicate mean ± standard deviation), showing a histogram of R_i and R_o. (**f**) Population data for 129 microtubule segments from one culture (mean ± standard deviation), showing a histogram of R_o-R_i.

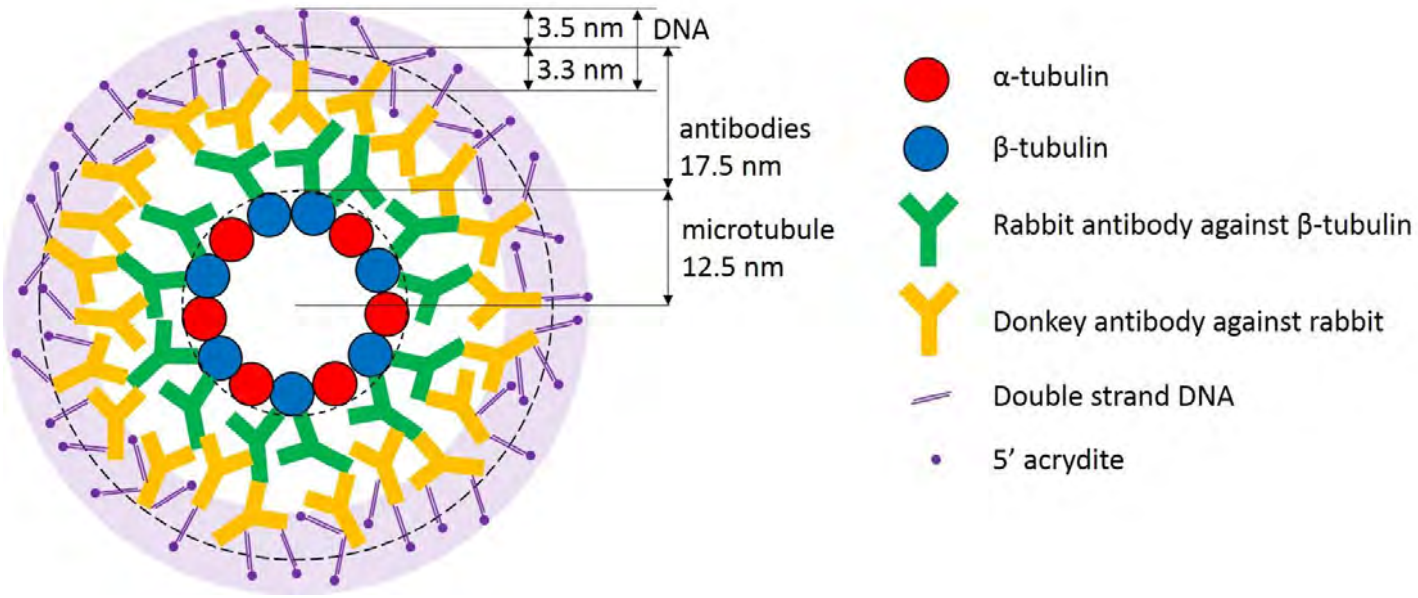

Supplementary Figure 3

Schematic of antibodies and DNA around a microtubule.

The 5' acrydites of the DNA oligos are distributed in the purple shaded region (corresponding to the cylinder of **Supplementary Fig. 2a**). We constructed a detailed schematic showing a possible arrangement of antibodies and DNA around microtubules, building from **Supplementary Fig. 2**. As shown in **Supplementary Fig. 3**, the radius of the microtubule is 12.5 nm, as previously measured by transmission electron microscopy (TEM)[1]. The radius of an immunostained microtubule (stained with conventional primary and secondary antibodies) is 30 nm, as measured by previous TEM imaging[1]. The 5' acrydites of the DNA are distributed in a cylinder with an inner radius of 26.7 nm and outer radius of 33.5 nm, as derived in **Supplementary Fig. 2e**. As can be seen in **Supplementary Fig. 3**, the DNA-conjugated secondary antibody makes the radius of the microtubule 3.5 nm larger than the microtubule labeled with regular antibodies (outer radius of 30 nm).

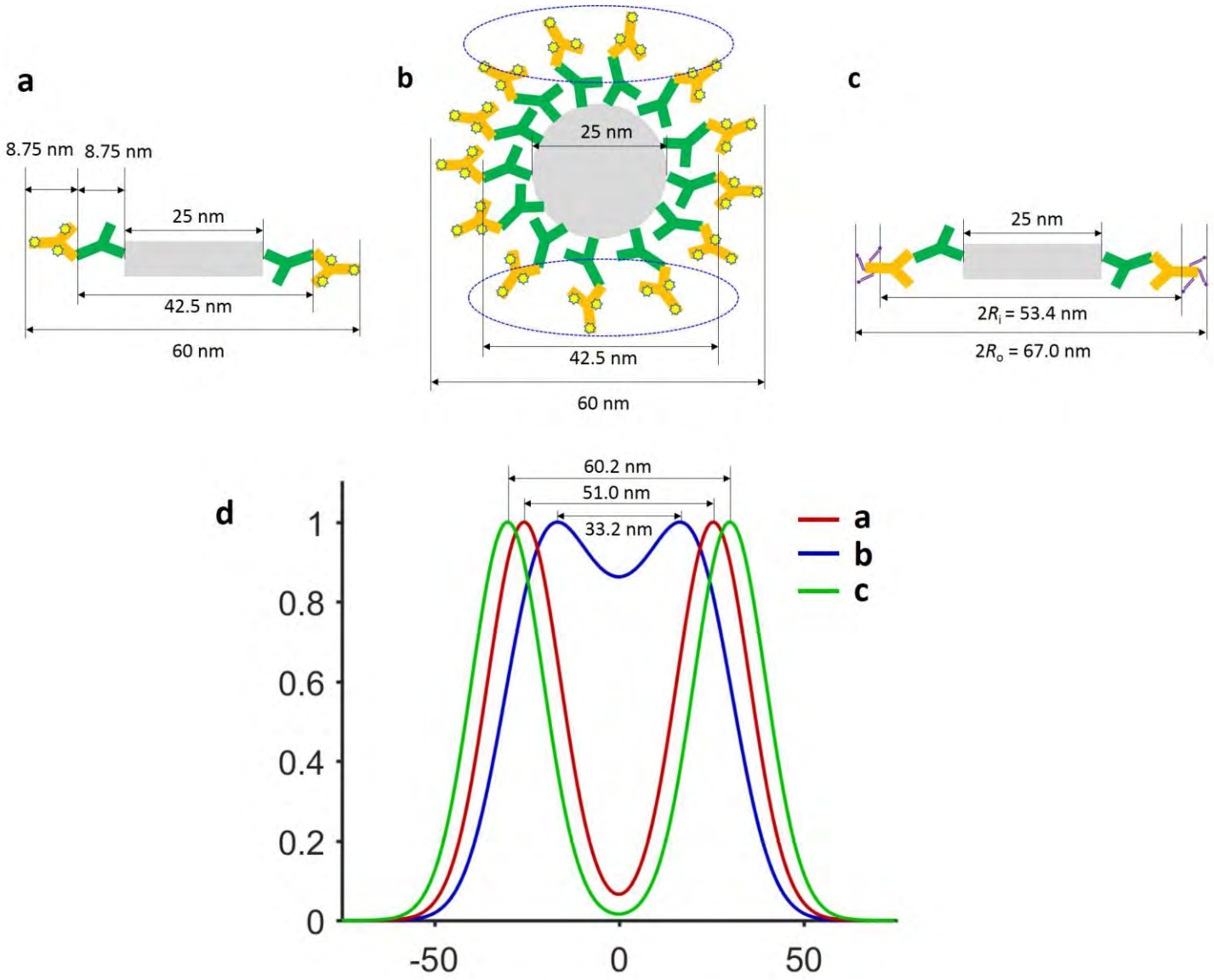

Supplementary Figure 4

Example of how antibody-bearing microscopy images differ as a function of the geometry of target protein complexes and the size of probes.

See **Supplementary Note 3** for related results text. (**a**) Cross section of a rectangular protein complex of interest, with an end-to-end length of 25 nm, and immunolabeled at the two lateral ends. (**b**) Cross section of a cylindrical protein complex of interest with a diameter of 25 nm, labeled from all sides. (**c**) Cross section of the same protein complex as in **a**, but labeled with a DNA-conjugated secondary antibody. Panel **a** and **c** show examples in which primary antibodies (green) bind only to the left and right surfaces of the protein complex. In panel **a**, fluorophore (yellow star)-labeled secondary antibodies (orange) are used. In panel **c**, DNA (purple line)-conjugated secondary antibodies (orange) are used. (**d**) The resulting fluorescence signal profiles (modeled by convolving the patterns of panels **a-c** with a FWHM of 22.8 nm, the point-spread function (PSF) of iExM excluding the label size (**Supplementary Fig. 6b**)) approximate how a small object might look when labeled with conventional antibodies (panel **a** and **b**) or DNA-conjugated antibodies (panel **c**) imaged via a super-

resolution technique with a resolution of 22.8 nm (such as iExM).

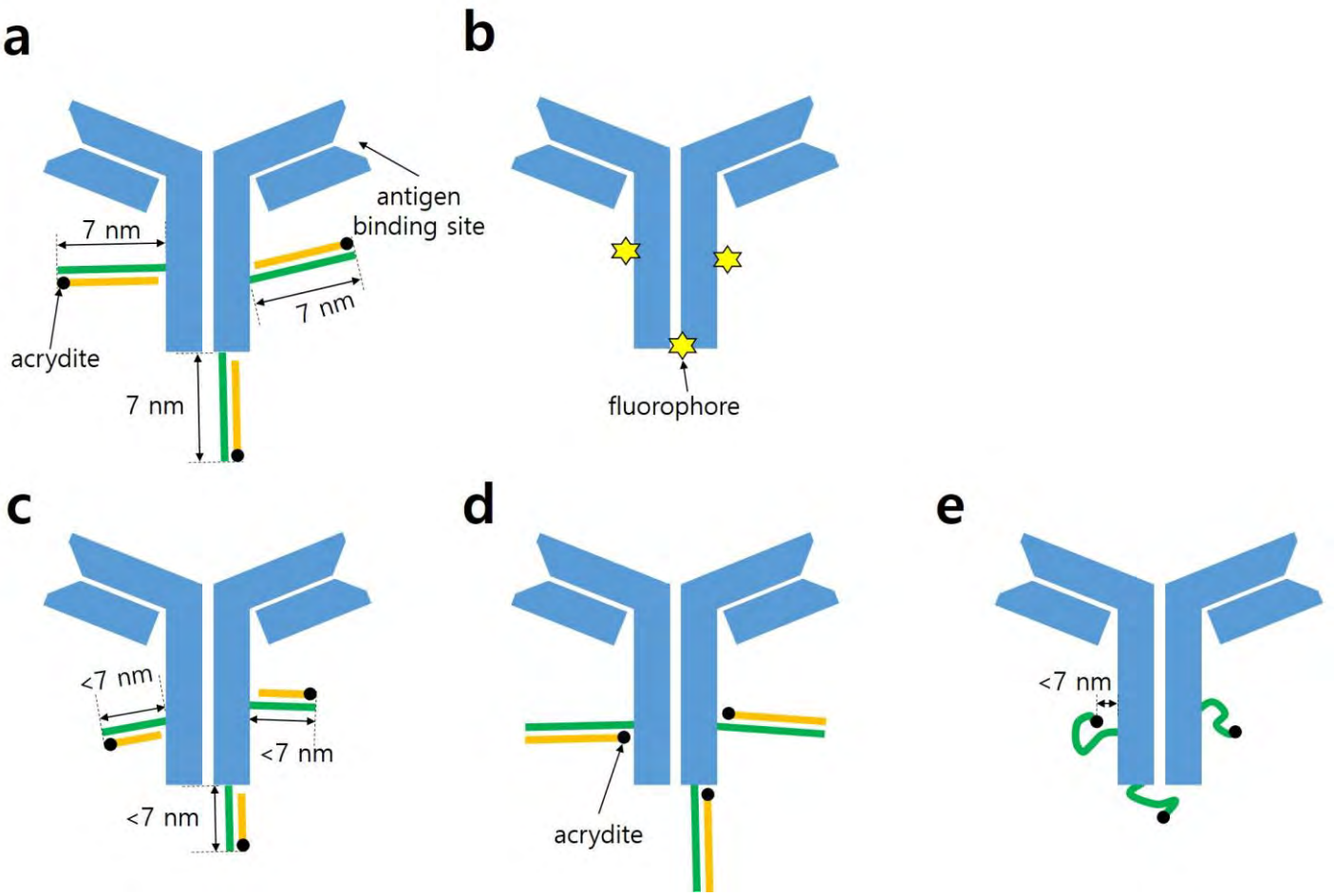

Supplementary Figure 5

iExM secondary antibodies with a smaller effective probe size.

See **Supplementary Note 4** for associated results text. (**a**) Schematic of the DNA-conjugated secondary antibody used in this study. (**b**) Schematic of a regular secondary antibody bearing fluorophores. (**c-e**), Three possible designs of DNA-conjugated secondary antibodies with a smaller size. (**c**) A shorter strand of DNA is used. (**d**) The acrydite (i.e., gel anchoring group) is positioned at the proximal end of the DNA. (**e**) A single stranded DNA with an acrydite moiety is conjugated to a secondary antibody.

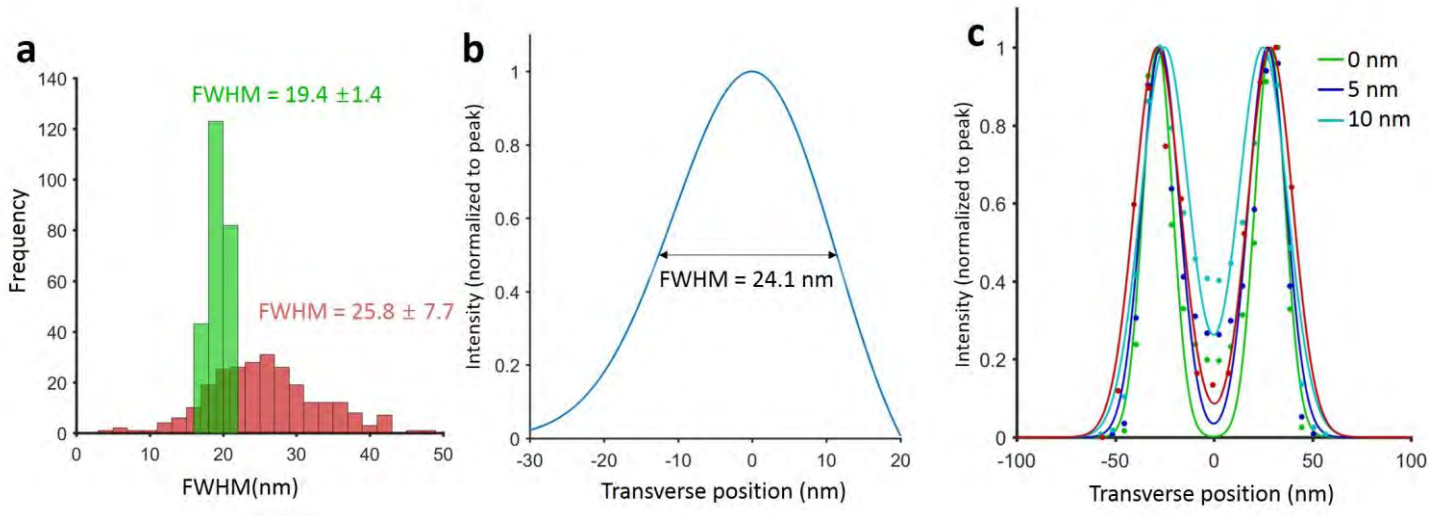

Supplementary Figure 6

Resolution measurement.

See **Supplementary Note 5** for associated results text. (**a**) Population data for 129 microtubules from one culture (two such sidewalls were obtained from each microtubule, for a total of 258 individual sidewalls), showing a histogram of the full width at half-maximums (FWHMs) of these single sidewalls (examples of such FWHMs are shown in **Supplementary Fig. 2c** and 2**d** by green and red numbers). Green, FWHMs of simulated (according to the model of **Supplementary Fig. 2a**) microtubule profiles, as shown in green in **Supplementary Fig. 2c** and **2d**. Red, FWHMs of experimental microtubule profiles, as shown in red in **Supplementary Fig. 2c** and **d**. This is the "overall point spread function (PSF)" of iExM, which includes contributions to the PSF from the labels (primary and DNA oligo-conjugated secondary antibody), gelation and expansion steps, and optical diffraction. (**b**) A PSF of iExM, generated by deconvolving the experimental microtubule profile of **Supplementary Fig. 2c** with a simulated microtubule labeled with DNA-conjugated antibodies (simulated as in **Supplementary Fig. 3**, and not including the effects of optical diffraction), that isolates the gelation, expansion, and optical contributions to the PSF (that is, omitting the label contributions). (**c**) As in **Supplementary Fig. 2c**, but simulating additional 5 and 10 nm positional errors.

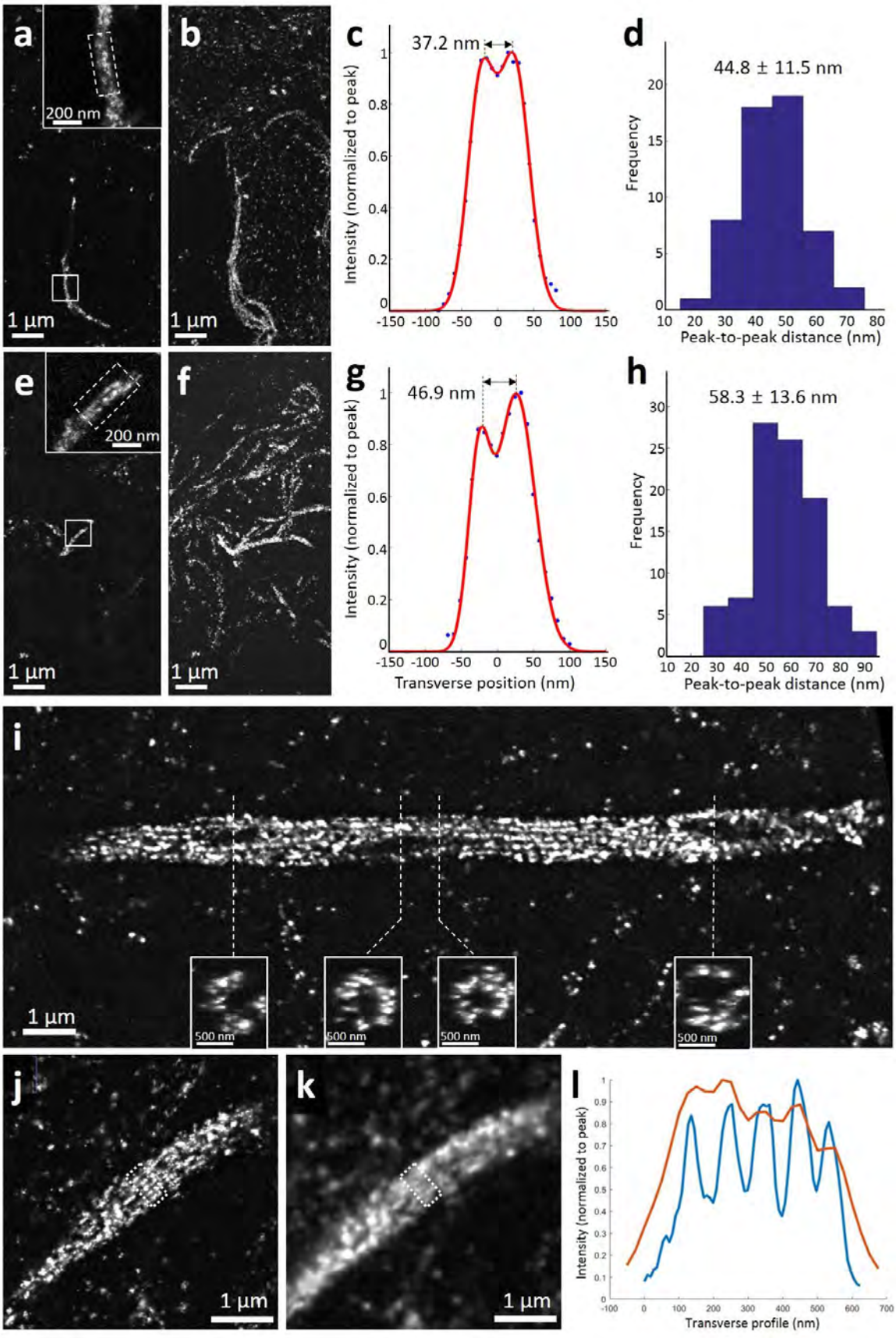

Nature Methods: doi:10.1038/nmeth.4261

Supplementary Figure 7

Imaging of microtubules of mouse lung, liver, and brain by iExM.

(**a**) Confocal microscopy image of microtubules of a 100-μm slice of preserved mouse lung tissue after 22-fold expansion by iExM. Inset zooms in the boxed area in **a**. (**b**) Maximum intensity projection of the sample imaged in **a**. (**c**) Transverse profile of the microtubules of the inset of **a** (blue dots), with superimposed fit with a sum of two Gaussians (red line). (**d**) Population data for 55 microtubule segments from one expanded sample, showing a histogram of the peak-to-peak distances. (**e**-**h**) As in **a**-**d**, but for a 100-μm thick slice of preserved mouse liver after 19-fold expansion. (**h**) 95 microtubule segments from one expanded sample were analyzed. (**i**) Representative image of microtubule bundles observed in mouse brain cells (cortex). The mouse cortex was immunostained with an antibody against tubulin and expanded 18-fold using iExM. z-stack images were acquired and the cross-sectional views shown in the bottom panels were constructed. (**j**) Confocal microscopy image of a microtubule bundle after 18-fold expansion. (**k**) Confocal microscopy image of the same microtubule bundle shown in **j** after shrinking the gel back to 6.5-fold in a salt solution, resulting in a resolution more similar to earlier ExM versions (~4.5-fold). (**l**) Transverse profiles of microtubules in the boxed regions of **j** and **k** (blue: **j**, orange: **k**).

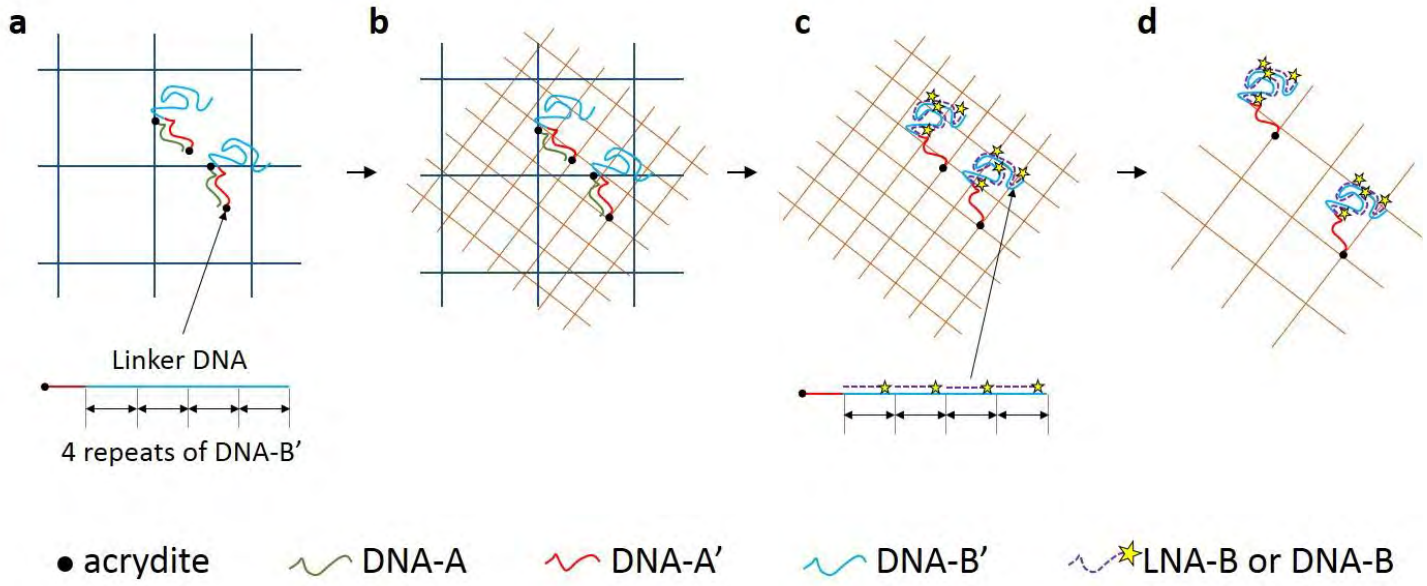

Supplementary Figure 8

Schematic of signal amplification based on DNA and locked nucleic acid (LNA).

See **Supplementary Note 7** for associated results text. (**a**) After the first hydrogel (dark blue) is expanded and re-embedded in an uncharged polyacrylamide gel (not shown), a long DNA (we call it 'linker DNA', schematized in the bottom left), consisting of the A' sequence (red) followed by four repeats of a new sequence B' (light blue), and equipped with a polymerizable group (black dot), is hybridized to the anchored DNA (green strand). (**b**) The second swellable hydrogel (orange) is formed, incorporating the new linker DNA strand. (**c**) DNA or LNA with a sequence of B (purple dotted line) with a fluorophore (yellow star) is hybridized to the linker DNA, enabling more fluorophores to be appended to the site of a given biomolecule. (**d**) The second gel is expanded in 0.2x PBS for DNA and in distilled (DI) water for LNA.

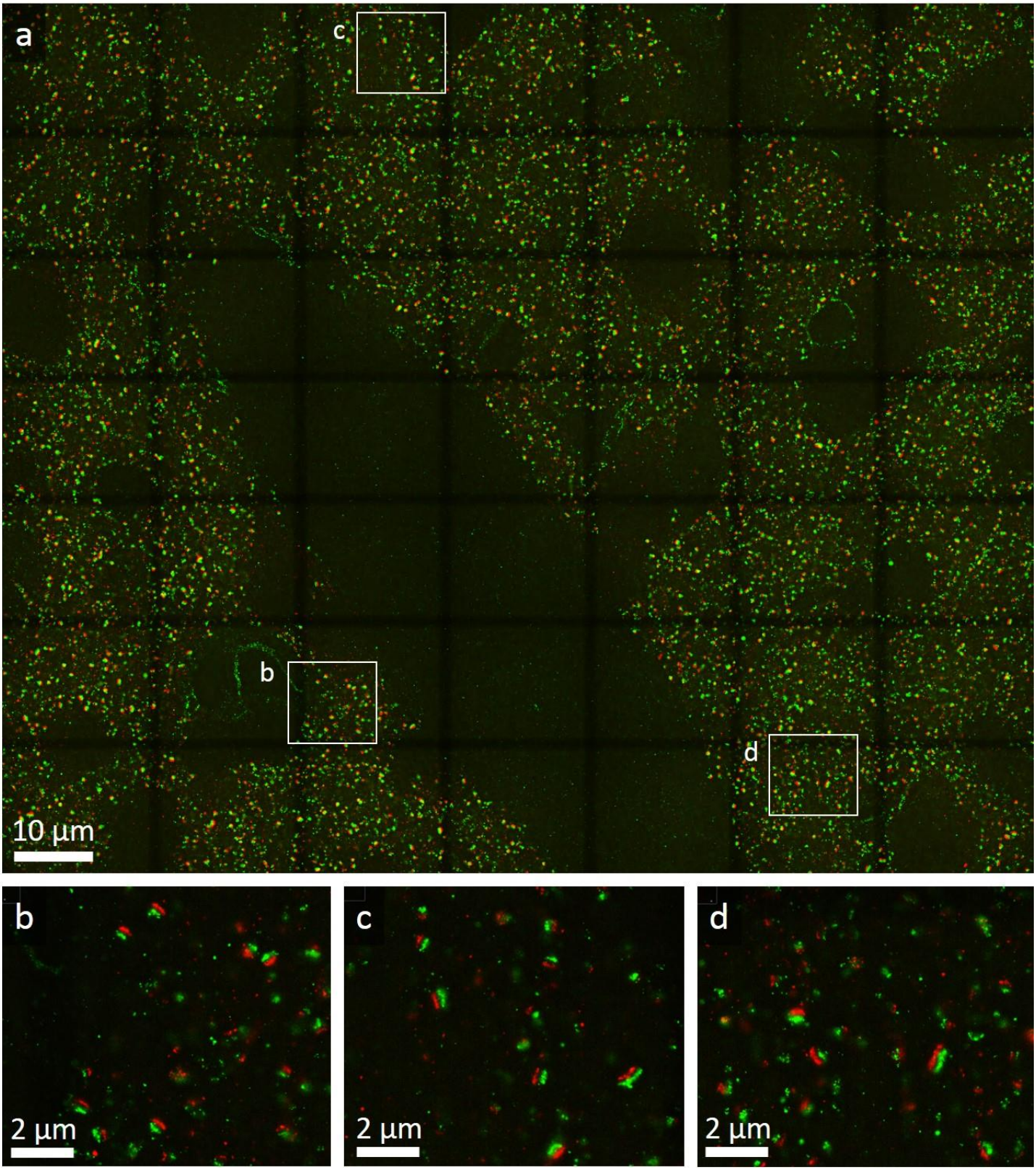

Supplementary Figure 9

Nature Methods: doi:10.1038/nmeth.4261

Large-area tiled epifluorescence image of Homer1 and Bassoon.

Epifluorescence image of Emx1-Cre mouse cortex labeled with anti-Homer1 (green) and anti-Bassoon (red), after 18-fold expansion via iExM and LNA hybridization-based signal amplification. Lower panels show magnified views of boxed regions in the upper panel.

Nature Methods: doi:10.1038/nmeth.4261

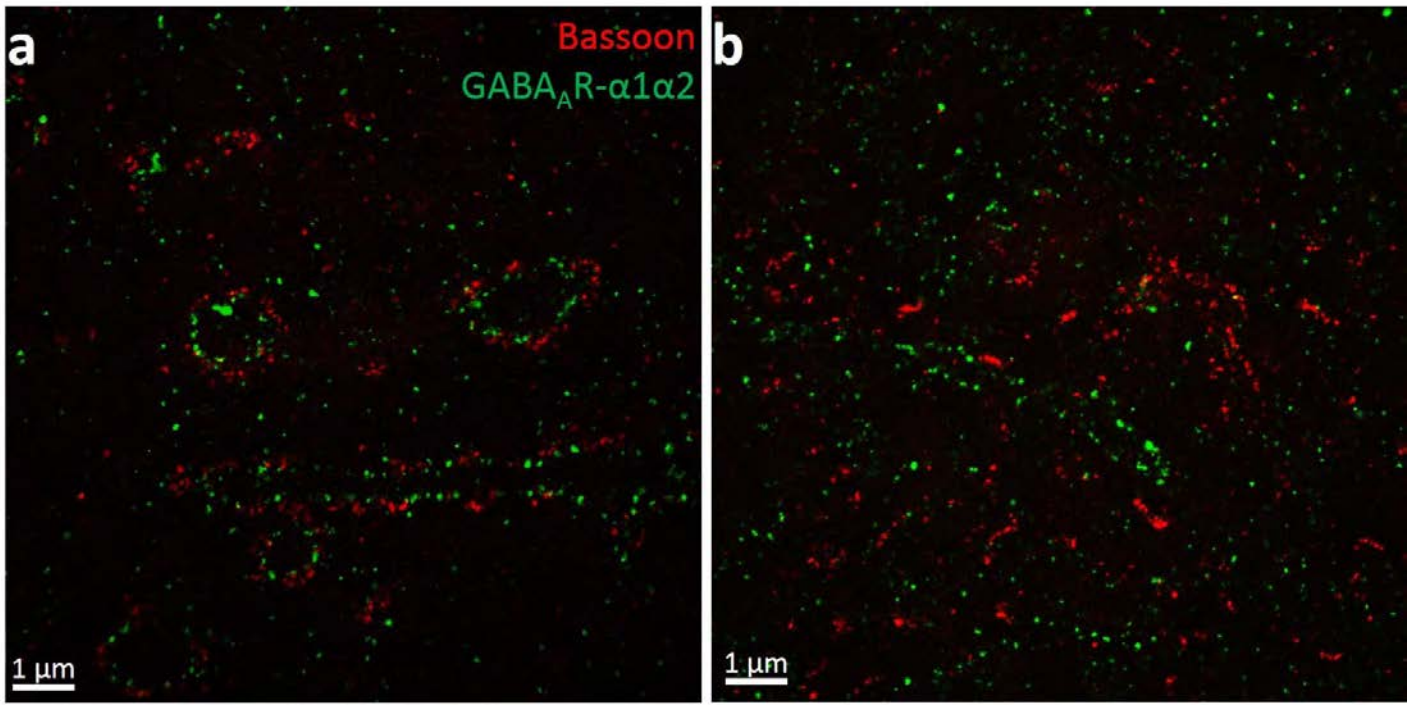

Supplementary Figure 10

Confocal images of two brain regions stained with anti-Bassoon and anti-GABA$_A$Rα1/α2.

Brain region: **a**, globus pallidus; **b**, cortex. Brains were expanded 16-fold via iExM. See **Supplementary Video 4** for 3-D movie of **a**.

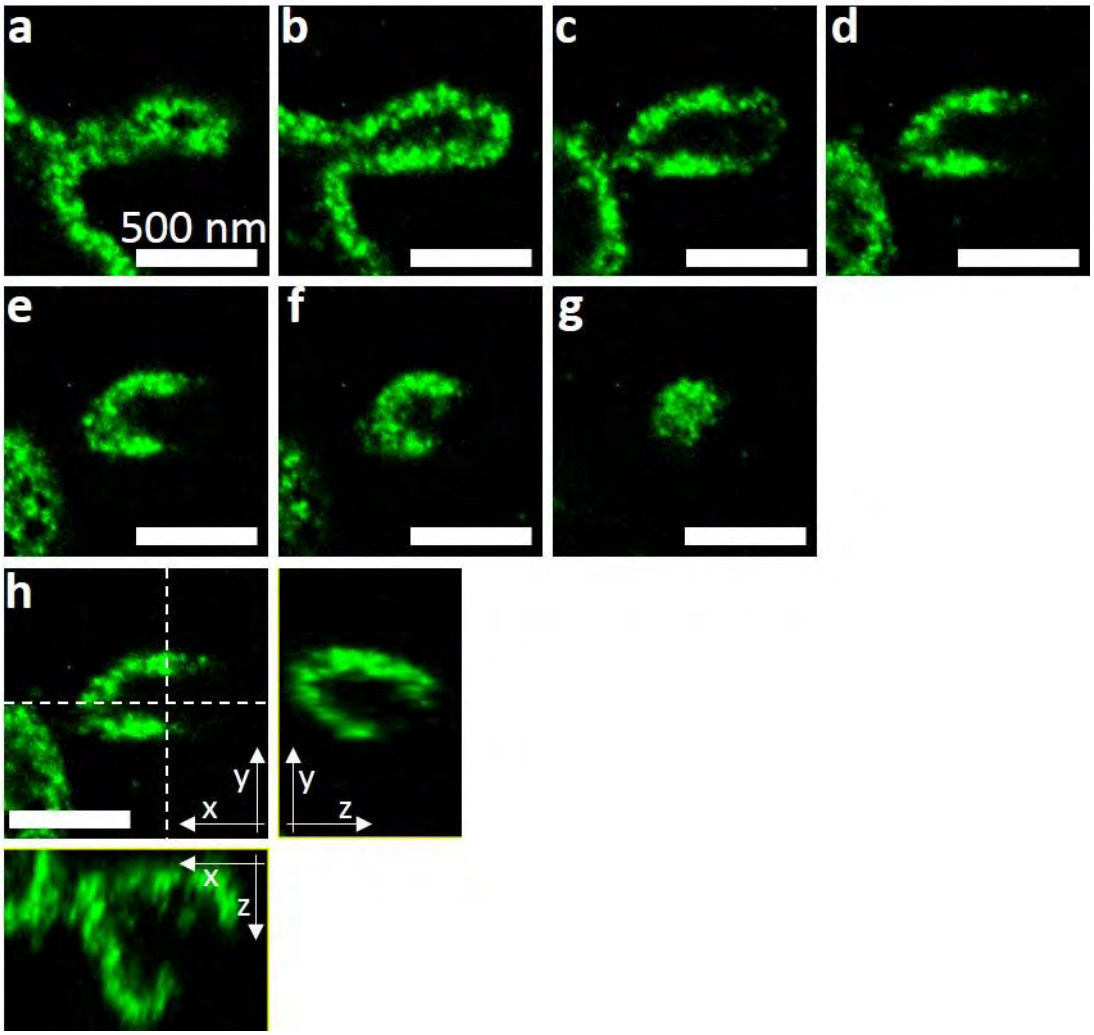

Supplementary Figure 11

Detailed view of the dendritic spine shown in Fig 4f.

(**a-g**) Single xy-plane images of the boxed region of **Fig. 3iv** at different z-heights. (**a**) z=3.05 μm. (**b**) z=3.15 μm. (**c**) z=3.28 μm. (**d**) z=3.33 μm. (**e**) z=3.38 μm. (**f**) z=3.42 μm. (**g**) z=3.55 μm. (**h**) Upper left shows a single xy-plane image at a z-height of 3.33 μm (same with **d**); right shows a single yz-plane image reconstructed from the z-stack image; bottom shows a single xz-plane image reconstructed from the z-stack image; dotted lines of upper left show the single x plane and y plane shown in the right and bottom. Scale bar = 500 nm.

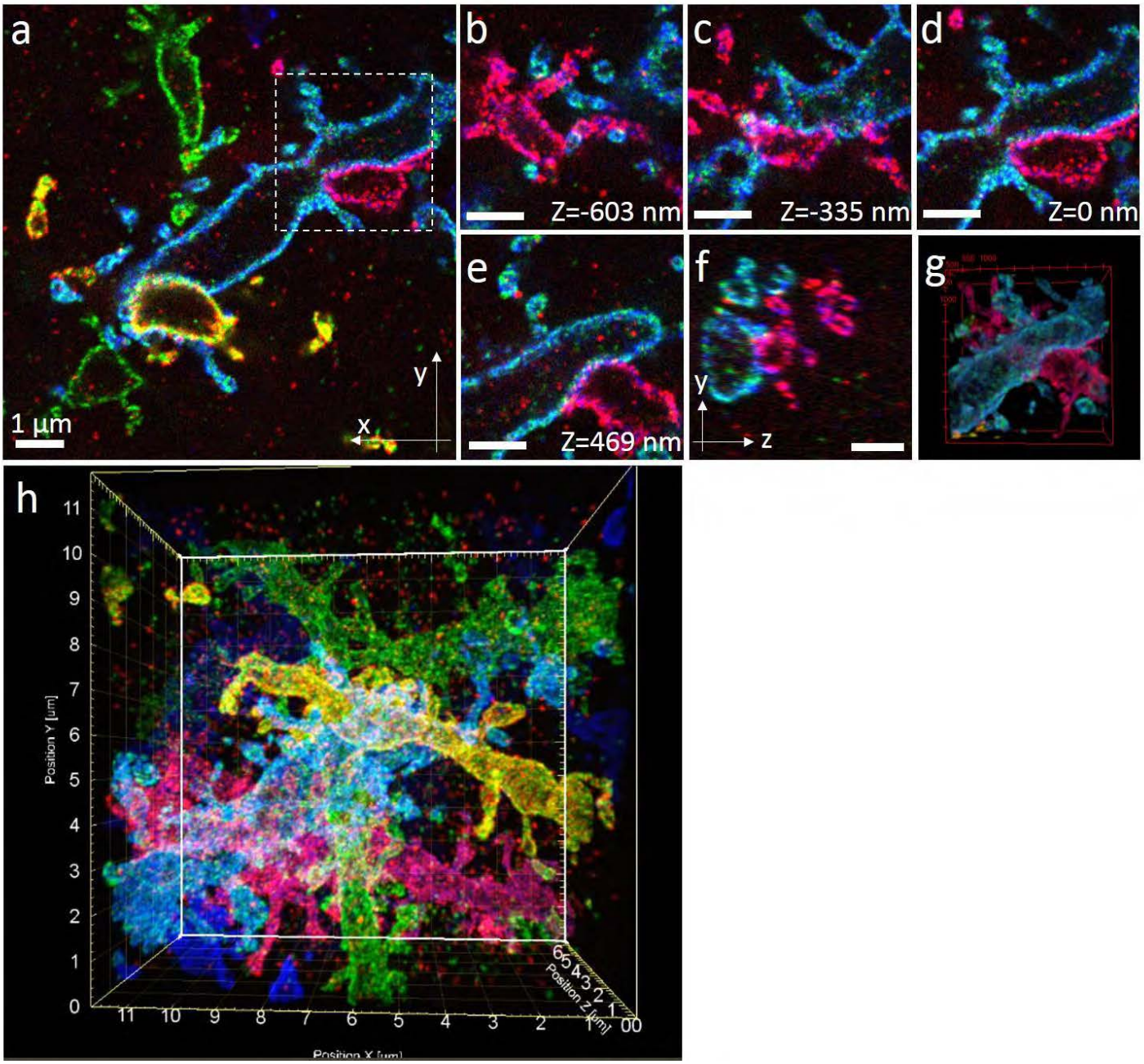

Supplementary Figure 12

Confocal image of 16-fold expanded Brainbow hippocampus.

16-fold expanded hippocampal brain circuitry with labeled mTFP (blue), mCherry (green), TagBFP (red). mCherry (green) signals and TagBFP (red) signals were amplified by LNA hybridization-based amplification. mTFP (blue) signals were not amplified. (**a**) Single confocal xy-plane image; (**b-e**) single xy-plane images at, and flanking (i.e., at different z-heights above and below the xy-plane of), the boxed region of **a**. (**f**) Single yz-plane image reconstructed from the z-stack images shown in **b-e**. Scale bar = 1 µm. (**g**) 3-D visualization of the volume shown in **b-e**. (**h**) 3-D visualization of the z-stack shown in **a**. See **Supplementary Video 6**.

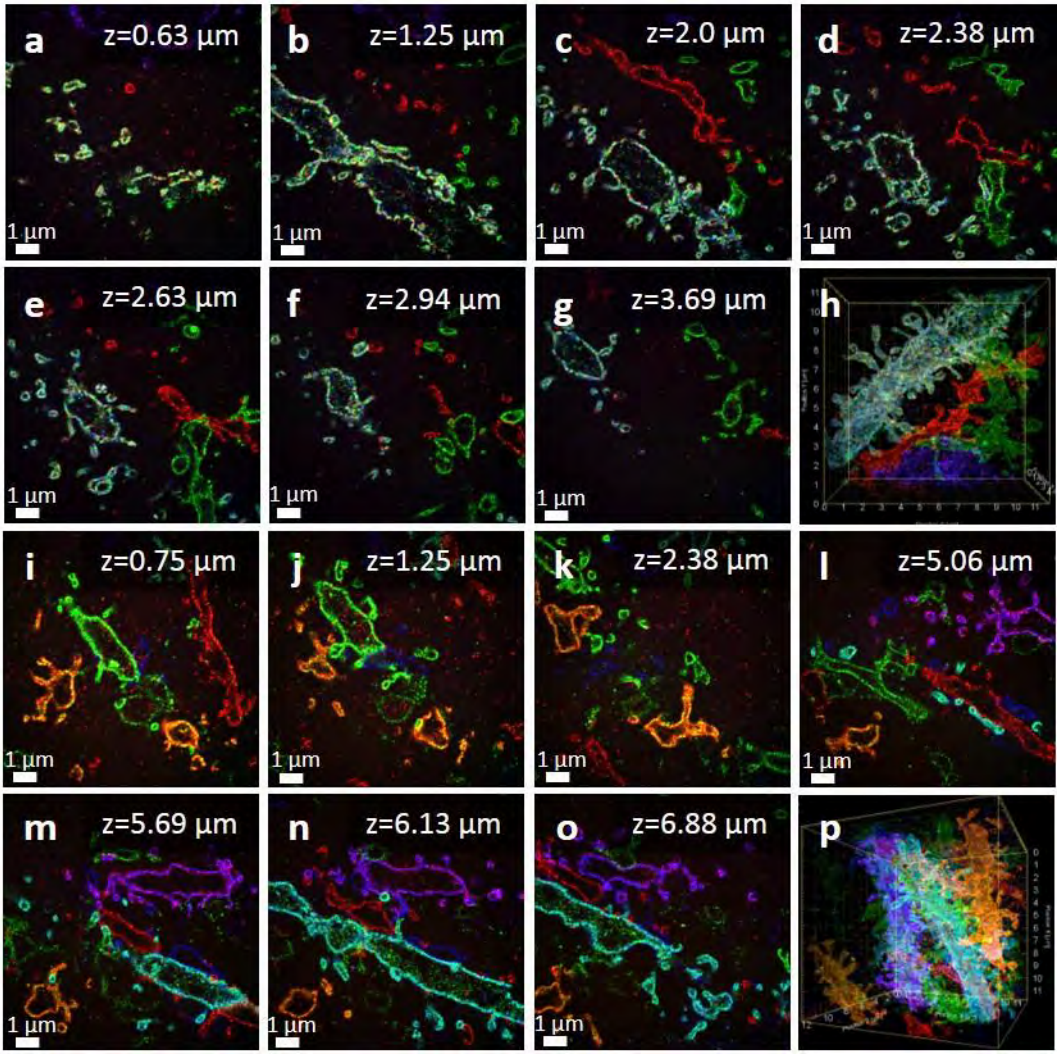

Supplementary Figure 13

Two confocal images of 16-fold expanded Brainbow hippocampus.

Two confocal z-stack images of 16-fold expanded mouse hippocampal circuitry with labeled mTFP (blue), mCherry (green), TagBFP (red). mCherry (green) signals and TagBFP (red) signals were amplified by LNA hybridization-based amplification. mTFP (blue) signals were not amplified. (**a**-**g**) Single xy-plane images at different z-heights. (**h**) Snapshot of a 3-D visualization of the z-stack shown in **a**-**g**; see **Supplementary Video 8**. (**i**-**o**) Single xy-plane images at different z-heights. (**p**) Snapshot of a 3-D visualization of the z-stack shown in **i**-**o**; see **Supplementary Video 9**.

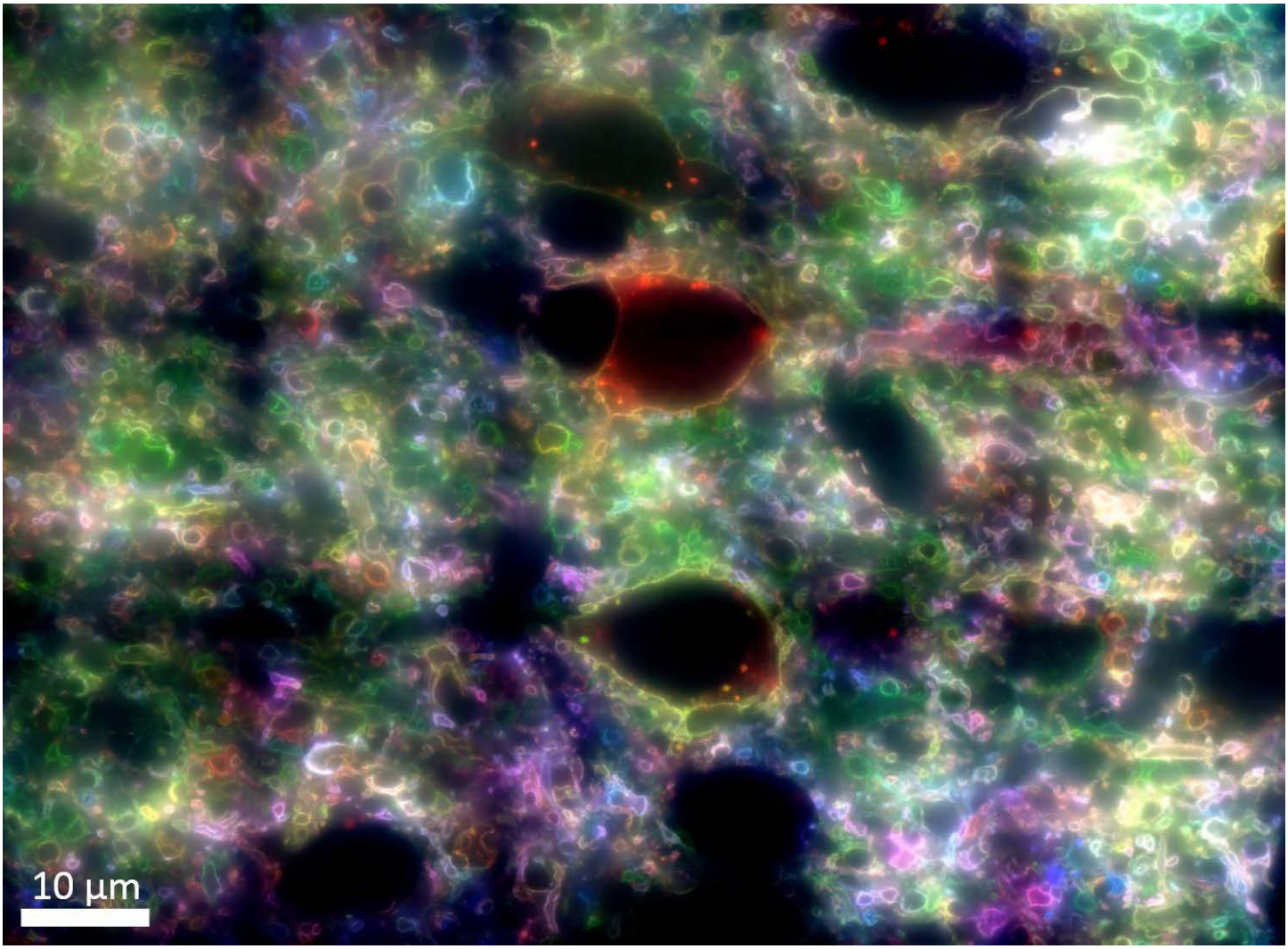

Supplementary Figure 14

Large-area tiling epifluorescence image of Emx1-Cre mouse cortex expressing membrane-bound fluorescent proteins (Brainbow AAVs).

TagBFP (green), mCherry (red), and EYFP (blue) were immunostained, expanded 16-fold via hp-iExM. TagBFP (green) and mCherry (red) signals were amplified by LNA hybridization-based signal amplification; EYFP (blue) signals were not amplified.

Nature Methods: doi:10.1038/nmeth.4261

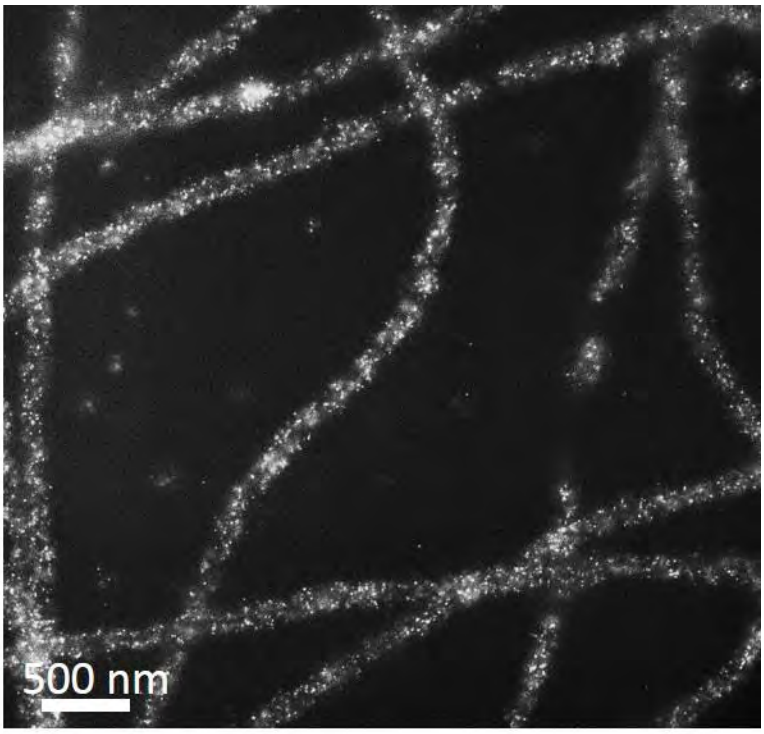

Supplementary Figure 15

Epifluorescence image of 53-fold expanded microtubules.

Epifluorescence image of cultured BS-C-1 cells labeled with anti-tubulin, and expanded ~53-fold via three consecutive expansions. Signal was amplified by LNA hybridization-based signal amplification. Associated results in **Supplementary Note 8**.

Nature Methods: doi:10.1038/nmeth.4261

Supplementary Table 1. List of chemicals

Product Name	Vendor	Product number
Gelation		
Sodium acrylate	Sigma	408220
Acrylamide	Sigma	A9099
N,N′-Methylenebisacrylamide (BIS)	Sigma	M7279
Ammonium Persulfate (APS)	Sigma	A3678
N,N,N′,N′-Tetramethylethylenediamine (TEMED)	Sigma	T7024
4-Hydroxy-TEMPO (H-tempo)	Sigma	176141
N,N'-(1,2-Dihydroxyethylene)bisacrylamide (DHEBA)	Tokyo Chemical Industry	D2864
N,N'-Cystaminebisacrylamide (BAC)	Polysciences	09809
Tris(2-carboxyethyl)phosphine (TCEP)	Sigma	646547
Cell and neuron culture		
Eagle's Minimum Essential Medium (EMEM)	American Type Culture Collection	30-2003
Fetal Bovine Serum	Corning	35-010-CV
Penicillin-Streptomycin Solution	Corning	30-002-CI
Fixation and staining		
Paraformaldehyde	Electron Microscopy Sciences	15710
Glutaraldehyde	Electron Microscopy Sciences	16020
Triton X-100	Sigma	X100
Glycine	Sigma	50046
PBS 10x	Life Technologies	70011-044
Dextran Sulfate 50%	Millipore	S4030
SSC 20x	Life Technologies	15557
Yeast tRNA	Roche	10109495001
Normal Donkey Serum	Jackson ImmunoResearch	017-000-001
1,4-Piperazinediethanesulfonic acid (PIPES)	Sigma	P1851
Ethylene glycol-bis(2-aminoethylether)-N,N,N′,N′-tetraacetic acid (EGTA)	Sigma	E38889
Magnesium chloride	Sigma	M8266
Digestion		
Proteinase K	New England Biolabs	P8107S
Ethylenediaminetetraacetic acid	Sigma	EDS
Guanidine HCl	Sigma	G3272
Tris-HCl, 1M pH 8.0	Life Technologies	AM9855
STORM imaging		
β-Mercaptoethanol	Sigma	M3148
Glucose oxidase	Sigma	G2133
Catalase	Sigma	C100
Glucose	Sigma	G7528

Supplementary Table 2. DNA with a 5'amine modification

Name	Sequence	Modifications
A1' 5'amine	AA CCG AAT ACA AAG CAT CAA CG	5'Amine
A2' 5'amine	AA GGT GAC AGG CAT CTC AAT CT	5'Amine
A3' 5'amine	AA GTC CCT GCC TCT ATA TCT CC	5'Amine
B1' 5'amine	AA TAC GCC CTA AGA ATC CGA AC	5'Amine
C1' 5'amine	AA GAC CCT AAG CAT ACA TCG TC	5'Amine

Nature Methods: doi:10.1038/nmeth.4261

Supplementary Table 3. DNA bearing a gel-anchoring moiety

Name	Sequence	Modifications
A1 5'acrydite 3'alexa488	CG TTG ATG CTT TGT ATT CGG T	5'Acrydite 3'Alexa488
A2 5'acrydite	AG ATT GAG ATG CCT GTC ACC	5'Acrydite
A3 5'acrydite	GG AGA TAT AGA GGC AGG GAC	5'Acrydite
B1 5'acrydite	GT TCG GAT TCT TAG GGC GTA	5'Acrydite
C1 5'acrydite	GA CGA TGT ATG CTT AGG GTC	5'Acrydite

Supplementary Table 4. DNA for 2nd expansion (no signal amplification)

Name	Sequence	Modifications
A1' 5'acrydite 3'atto565	CCG AAT ACA AAG CAT CAA CG	5'Acrydite 3'Atto565
C1' 5'acrydite 3'alexa488	GAC CCT AAG CAT ACA TCG TC	5'Acrydite 3'Alexa488

Supplementary Table 5. Linker DNA for DNA hybridization-based signal amplification (see Supplementary Fig. 10)

Name	Sequence	Modifications
A3' 4A1' 5'acrydite	GT CCC TGC CTC TAT ATC TCC ATA CCG AAT ACA AAG CAT CAA TAC CGA ATA CAA AGC ATC AAT ACC GAA TAC AAA GCA TCA ATA CCG AAT ACA AAG CAT CA	5'Acrydite
B1' 4B2' 5'acrydite	AT ACG CCC TAA GAA TCC GAA ATA GCA TTA CAG TCC TCA TAA TAG CAT TAC AGT CCT CAT AAT AGC ATT ACA GTC CTC ATA ATA GCA TTA CAG TCC TCA TA	5'Acrydite
C1' 4C2' 5'acrydite	AG ACC CTA AGC ATA CAT CGT ATA GAC TAC TGA TAA CTG GAA TAG ACT ACT GAT AAC TGG AAT AGA CTA CTG ATA ACT GGA ATA GAC TAC TGA TAA CTG GA	5'Acrydite

Supplementary Table 6. Fluorophore-tagged DNA for DNA hybridization-based signal amplification (See Supplementary Fig. 10)

Name	Sequence	Modifications
A1 3'alexa488	CG TTG ATG CTT TGT ATT CGG T	3'Alexa488
B2 3'atto565	ACT TAT GAG GAC TGT AAT GCT	3'Atto565
C2 3'atto647N	CAA TCC AGT TAT CAG TAG TCT	3'Atto647N

Supplementary Table 7. Linker DNA for LNA hybridization-based signal amplification (see Supplementary Fig. 10)

Name	Sequence	Modifications
A2' 4LNA-A1' 5'Acrydite	GG TGA CAG GCA TCT CAA TCT ATT ACA AAG CAT CAA CGA TTA CAA AGC ATC AAC GAT TAC AAA GCA TCA ACG ATT ACA AAG CAT CAA CG	5'Acrydite
A3' 4LNA-A1' 5'Acrydite	GT CCC TGC CTC TAT ATC TCC ATT ACA AAG CAT CAA CGA TTA CAA AGC ATC AAC GAT TAC AAA GCA TCA ACG ATT ACA AAG CAT CAA CG	5'Acrydite
B1' 4LNA-B2' 5'Acrydite	TA CGC CCT AAG AAT CCG AAC ATG CAT TAC AGC CCT CAA TGC ATT ACA GCC CTC AAT GCA TTA CAG CCC TCA ATG CAT TAC AGC CCT CA	5'Acrydite

Supplementary Table 8. DNA for triple round expansion

Name	Sequence	Modifications
B1' A2 5'acrydite	TA CGC CCT AAG AAT CCG AAC ATA GAT TGA GAT GCC TGT CAC C	5'Acrydite

Nature Methods: doi:10.1038/nmeth.4261

Supplementary Table 9. Fluorophore-tagged LNA for LNA hybridization-based signal amplification (see Supplementary Fig. 10) (underlined letters: LNA)

Name	Sequence	Modifications
LNA-A1 3'Atto565	CGTTGATGCTTTGTA	3'Atto565
LNA-B2 3'Atto647N	TGAGGGCTGTAATGC	3'Atto647N

Nature Methods: doi:10.1038/nmeth.4261

Supplementary Table 10. Immunostaining and DNA hybridization condition

(except **Supplementary Fig. 15**; see '**7. Triple round expansion**' of Methods)

Figure	Imaging method	Primary antibody	Secondary antibody	DNA hybridization after 2nd antibody staining	DNA hybridization after re-embedding	DNA hybridization after 2nd swellable gel synthesis
Main Text Figures						
2a-c	STORM	anti-beta Tubulin (rb)	anti-Rb alexa647			
2d-n	iExM	anti-beta Tubulin (rb)	RbA1'	A1 5'acrydite 3'alexa488	A1' 5'acrydite 3'atto565	
2o,p	STORM/iExM	anti-beta Tubulin (rb)	RbA1' anti-Rb alexa647	A1 5'acrydite 3'alexa488	A1' 5'acrydite 3'atto565	
3a-c	iExM	anti-GluR1 (rb) anti-Basson (ms) anti-Homer1 (gp)	RbA3' MsB1' GpC1'	A3 5'acrydite B1 5'acrydite C1 5'acrydite	A3' 4A1' 5'acrydite B1' 4B2' 5'acrydite C1' 4C2' 5'acrydite	A1 3'alexa488 B2 3'atto565 C2 3'atto647N
3d-f	iExM	anti-GABARAα1/α2 (rb) anti-Gephyrin (ms) anti-Bassoon (gp)	RbA3' MsB1' GpC1'	A3 5'acrydite B1 5'acrydite C1 5'acrydite	A3' 4A1' 5'acrydite B1' 4B2' 5'acrydite C1' 4C2' 5'acrydite	A1 3'alexa488 B2 3'atto565 C2 3'atto647N
3g	iExM	anti-GluR1 (rb) anti-Homer1 (ms)	RbA2' MsB1'	A2 5'acrydite B1 5'acrydite	A2' 4LNA-A1' 5'acrydite B1' 4LNA-B2' 5'acrydite	LNA-A1 3'atto565 LNA-B2 3'atto647N
3i-s	iExM	anti-Homer1 (rb) anti-Bassoon (ms)	RbA2' MsB1'	A2 5'acrydite B1 5'acrydite	A2' 4LNA-A1' 5'acrydite B1' 4LNA-B2' 5'acrydite	LNA-A1 3'atto565 LNA-B2 3'atto647N
3t	iExM	anti-Homer1 (rb) anti-mCherry (rt)	RbA2' RtC1'	A2 5'acrydite C1 5'acrydite	A2' 4LNA-A1' 5'acrydite C1' 5'acrydite 3'alexa488	LNA-A1 3'atto565
3u	iExM	anti-Homer1 (rb) anti-GFP (chk)$^{+}$	RbA2' ChkC1'	A2 5'acrydite C1 5'acrydite	A2' 4LNA-A1' 5'acrydite C1' 5'acrydite 3'alexa488	LNA-A1 3'atto565
4a		anti-GFP (chk)$^{+}$ anti-mTFP (rt) anti-TagRFP (gp)*	anti-Chk alexa488 anti-Rt alexa546 anti-Gp CF633			
4b	ProExM	anti-GFP (chk)$^{+}$ anti-mTFP (rt) anti-TagRFP (gp)*	anti-Chk alexa488 anti-Rt alexa546 anti-Gp CF633			

Nature Methods: doi:10.1038/nmeth.4261

4c	iExM	anti-mCherry (rb) anti-TagRFP (gp)* anti-GFP (chk)+ anti-mTFP (rt)	RbA2' GpB1' ChkC1' RtC1'	A2 5'acrydite B1 5'acrydite C1 5'acrydite	A2' 4LNA-A1' 5'acrydite B1' 4LNA-B2' 5'acrydite C1' 5'acrydite 3'alexa388	LNA-A1 3'atto565 LNA-B2 3'atto647N
4d	iExM	anti-mCherry (rb) anti-TagRFP (gp)* anti-GFP (chk)+ anti-mTFP (rt)	RbA2' GpB1' ChkC1' RtC1'	A2 5'acrydite B1 5'acrydite C1 5'acrydite	A2' 4LNA-A1' 5'acrydite B1' 4LNA-B2' 5'acrydite C1' 5'acrydite 3'alexa388	LNA-A1 3'atto565 LNA-B2 3'atto647N
Supplementary Information Figures						
1	hp-iExM	anti-beta Tubulin	RbA1'	A1 5'acrydite 3'alexa488	A1' 5'acrydite 3'atto565	
2b	iExM	anti-beta Tubulin (rb)	RbA1'	A1 5'acrydite 3'alexa488	A1' 5'acrydite 3'atto565	
7	iExM	anti-beta Tubulin (rb)	RbA1'	A1 5'acrydite 3'alexa488	A1' 5'acrydite 3'atto565	
9	iExM	anti-Homer1 (rb) anti-Bassoon (ms)	MsA2' RbB1'	A2 5'acrydite B1 5'acrydite	A2' 4LNA-A1' 5'acrydite B1' 4LNA-B2' 5'acrydite	LNA-A1 3'atto565 LNA-B2 3'atto647N
10	iExM	anti-GABARAα1/α2 (rb) anti-Bassoon (ms)	RbA2' MsB1'	A2 5'acrydite B1 5'acrydite	A2' 4LNA-A1' 5'acrydite B1' 4LNA-B2' 5'acrydite	LNA-A1 3'atto565 LNA-B2 3'atto647N
11	same with **Fig. 4c**					
12,13	iExM	anti-mCherry (rb) anti-TagRFP (gp)* anti-mTFP (rt)	RbA2' GpB1' RtC1'	A2 5'acrydite B1 5'acrydite C1 5'acrydite	A2' 4LNA-A1' 5'acrydite B1' 4LNA-B2' 5'acrydite C1' 5'acrydite 3'alexa388	LNA-A1 3'atto565 LNA-B2 3'atto647N
14	hp-iExM	anti-TagRFP (gp)* anti-mTFP (rt) anti-GFP (chk)+	GpA2' RtB1' ChkC1'	A2 5'acrydite B1 5'acrydite C1 5'acrydite	A2' 4LNA-A1' 5'acrydite B1' 4LNA-B2' 5'acrydite C1' 5'acrydite 3'alexa388	LNA-A1 3'atto565 LNA-B2 3'atto647N

*anti-TagRFP antibody binds also to TagBFP.
+anti-GFP antibody binds also to EYFP.

Nature Methods: doi:10.1038/nmeth.4261

Supplementary Table 11. Primary and secondary antibody list

Primary/ Secondary	Target	Host*	Vendor**	Product number	Dilution
Primary	Beta tubulin	Rb	Abcam	ab6046	1:100
Primary	Homer1	Rb	SYSY	160003	1:200
Primary	Homer1	Gp	SYSY	160004	1:200
Primary	Homer1	Ms	SYSY	160011	1:200
Primary	Bassoon	Ms	Enzo	ADI-VAM-PS003-F	1:200
Primary	Bassoon	Gp	SYSY	141004	1:200
Primary	Gephyrin	Ms	SYSY	147011	1:200
Primary	$GABA_AR\alpha1$	Rb	SYSY	224203	1:200
Primary	$GABA_AR\alpha2$	Rb	SYSY	224103	1:200
Primary	GluR1	Rb	Abcam	ab31232	1:100
Primary	TagRFP	Gp	Kerafast/Cai lab	EMU107	1:200
Primary	mCherry	Rb	Abcam	ab167453	1:200
Primary	mCherry	Rt	ThermoFisher	M11217	1:200
Primary	mTFP	Rt	Kerafast/Cai lab	EMU103	1:200
Primary	GFP	Chk	Kerafast/Cai lab	EMU101	1:400
Secondary	Chicken	Gt	ThermoFisher	A-11039 (alexa 488 conjugated)	10 µg/uL
Secondary	Rat	Gt	ThermoFisher	A-11081 (alexa 546 conjugated)	10 µg/uL
Secondary	Guinea Pig	Gt	Biotium	Biotium (CF633 conjugated)	10 µg/uL
Secondary	Rabbit	Dk	JIR	711-005-152	10 µg/uL for cultured cells and cultured neurons and 20 µg/µL for brain slices
Secondary	Chicken	Dk	JIR	703-005-155	
Secondary	Rat	Dk	JIR	712-005-153	
Secondary	Guinea Pig	Dk	JIR	706-005-148	
Secondary	Mouse	Dk	JIR	715-005-151	
Secondary	Rabbit	Dk	ThermoFisher	A-31573 (alexa 647 conjugated)	1:100

*Host - Rb: rabbit, Ms: mouse, Gp: Guinea pig, Rt: Rat, Chk: Chicken, Gt: Goat, Dk: Donkey
**Vender – SYSY: Synaptic Systems, JIR: Jackson ImmunoRearch

Supplementary Table 12. DNA-conjugated secondary antibodies

Name	Host of 2nd antibody	Conjugated DNA
RbA1'	Rabbit	A1' 5'amine
RbA2'	Rabbit	A2' 5'amine
RbA3'	Rabbit	A3' 5'amine
RbB1'	Rabbit	B1' 5'amine
MsA2'	Mouse	A2' 5'amine
MsB1'	Mouse	B1' 5'amine
GpA2'	Guinea pig	A2' 5'amine
GpB1'	Guinea pig	B1' 5'amine
GpC1'	Guinea pig	C1' 5'amine
RtB1'	Rat	B1' 5'amine
RtC1'	Rat	C1' 5'amine
ChkC1'	Chicken	C1' 5'amine

Nature Methods: doi:10.1038/nmeth.4261

Supplementary Table 13. Gel solution of hp-iExM and iExM

	Pre-gel Incubation solution	1st gel solution	Re-embedding solution	hp-iExM 2nd gel solution	iExM 2nd gel solution
Sodium acrylate	8.625% (w/w)	8.625% (w/w)	0	0	8.625% (w/w)
Acrylamide	2.5% (w/w)	2.5% (w/w)	10% (w/w)	10% (w/w)	2.5% (w/w)
Crosslinker	DHEBA 0.2% (w/w)	DHEBA 0.2% (w/w)	DHEBA 0.2% (w/w)	BIS 0.15% (w/w)	BIS 0.15% (w/w)
APS	0	0.2% (w/w)	0.05% (w/w)	0.05% (w/w)	0.05% (w/w)
TEMED	0	0.2% (v/w)	0.05% (v/w)	0.05% (v/w)	0.05% (v/w)
NaCl	1.865M	1.865M	0	0	2M
PBS	1x	1x	0	0.15x	1x
H-tempo	0	0.005%	0	0	0
Incubation/gelation temperature	4 ºC	37 ºC	37 ºC	Room temperature	37 ºC
Incubation/gelation duration	Overnight (12 hours)	3 hours	1.5 hours	1.5 hours	1.5 hours

Supplementary Table 14. Gel solution for triple round expansion

	Pre-gel Incubation solution	1st gel solution	1st Re-embedding solution	2nd gel solution	2nd re-embedding solution	3rd gel solution
Sodium acrylate	8.625% (w/w)	8.625% (w/w)	0	8.625% (w/w)	0	8.625% (w/w)
Acrylamide	2.5% (w/w)	2.5% (w/w)	10% (w/w)	2.5% (w/w)	10% (w/w)	2.5% (w/w)
Crosslinker	BAC 0.2% (w/w)	BAC 0.2% (w/w)	BAC 0.2% (w/w)	DHEBA 0.2% (w/w)	DHEBA 0.2% (w/w)	BIS 0.15% (w/w)
APS	0	0.2% (w/w)	0.05% (w/w)	0.05% (w/w)	0.05% (w/w)	0.05% (w/w/)
TEMED	0	0.2% (v/w)	0.05% (v/w)	0.05% (v/w)	0.05% (v/w)	0.05% (v/w)
NaCl	1.11M	0.89M	0	2M	0	2M
PBS	1x	1x	0	1x	0	1x
H-tempo	0	0.005%	0	0	0	0
Incubation/Gelation temperature	4 ºC	37 ºC	37 ºC	37 ºC	37 ºC	37 ºC
Incubation/Gelation duration	Overnight (12 hours)	3 hours	1.5 hours	1.5 hours	1.5 hours	1.5 hours

Nature Methods: doi:10.1038/nmeth.4261

Supplementary Note 1. Expansion factor: We found that iExM would typically result in expansion ratios of ~4.5x (with 0.005% H-TEMPO inhibitor; see Methods for details) to ~5.5x (with 0.01% H-TEMPO) in the first round, and ~4x in the second round, for a total increase of ~16x-22x. hp-iExM resulted in ~4.5x (with 0.005% H-TEMPO) to ~5.5x (with 0.01% H-TEMPO) expansion ratios in the first round of expansion, followed by ~3.5x in the second round, for a total increase of ~14-19x.

Supplementary Note 2. Details of the iExM simulator: We developed a computer simulation of how microtubules would look when they were labeled with a primary antibody and a DNA-conjugated secondary antibody, and then expanded 20-fold via iExM (**Supplementary Fig. 2**). We first calculated the point spread function (PSF) of the microscope system we used (a spinning disk confocal microscope with a pinhole size of 50 μm equipped with a 40x NA1.15 objective lens), as shown in **Supplementary Fig. 2a**. We positioned points in a cylinder between two shells, with inner and outer radius R_i and R_o respectively. The points in the cylinder simulate the distribution of the 5' acrydites of the DNA anchored to the first polymer of iExM. This DNA is anchored to the hydrogel through its 5' acrydite, and then a complementary DNA with a fluorophore is finally hybridized to this gel-anchored DNA, for incorporation into the final gel. These points were randomly positioned inside the cylinder to simulate the stochastic nature of the antibody binding to its target protein. We then convolved the PSF with the points in the cylinder to construct a final image of a microtubule. See section 'MATLAB simulation of iExM images' of the Methods for details of calculating R_i and R_o. A simulated cylinder with an inner radius of the average R_i and outer radius of the average R_o (green dots, **Supplementary Fig. 2c, 2d**) was generated and super-imposed onto the experimental results (red dots). When we analyzed 129 microtubule segments (from one culture), the average R_i was 26.7 ± 5.6 nm (mean ± standard deviation) and the average R_o was 33.5 ± 2.1 nm, as shown in **Supplementary Fig. 2e**. The average thickness of the 5' acrydite layer was 6.8 ± 3.6 nm, as shown in **Supplementary Fig. 2f**.

Supplementary Note 3. Positional error of proteins labeled with DNA-conjugated secondary antibodies: We can (**Supplementary Fig. 4**) calculate the positional error when a DNA-conjugated secondary antibody is used instead of a regular secondary antibody to label a protein complex on two sides, as shown in **Supplementary Fig. 4c** and **d**. The peak-to-peak distance would be 60.2 nm (**Supplementary Fig. 4c** and green trace in **d**); taking the peak to be at the center of the DNA layer, estimated using the calculations of **Supplementary Fig. 2e,** or $2 \times (26.7+33.5)/2$), which is 9.2 nm larger than the peak-to-peak distance (51 nm) measured by immunostaining with regular secondary antibodies. So, the DNA-conjugated antibody adds 4.6 nm (9.2/2=4.6 nm per epitope) of positional error to a protein complex vs. when labeled with regular secondary antibodies if the antibodies bind to the target protein asymmetrically, as in **Supplementary Figure Fig. 4a** and **d**.

Nature Methods: doi:10.1038/nmeth.4261

Supplementary Note 4. New probe designs with a smaller probe size: In our experiments, a secondary antibody conjugated with a 7-nm long strand of DNA was used (**Supplementary Fig. 5a**). As this DNA-antibody complex is larger than a regular secondary antibody (**Supplementary Fig. 5b**), the use of a DNA-conjugated antibody adds another 4.6 nm positional error to a typical measurement, as discussed in **Supplementary Fig. 4**. We schematized (**Supplementary Fig. 5**) three options to make the DNA-conjugated secondary antibody smaller. First, a shorter strand of DNA could be used (**Supplementary Fig. 5c**). To prevent the melting of shorter double strand DNA oligos, a buffer with a higher salt concentration could be used. Second, the position of an acrydite moiety could be changed from the far end of the DNA to the proximal end (**Supplementary Fig. 5d**). Thirdly, a single stranded DNA oligo with an acrydite moiety could be conjugated to the secondary antibody directly. As the persistence length of single stranded DNA is much shorter than double stranded DNA[2], the distance from the surface of the secondary antibody to the acrydite would be shorter than the current design (**Supplementary Fig. 5e**). All three options presented here use only commercially available reagents, and would not require additional modification to the current iterative expansion microscopy protocol. To minimize such positional errors further, one could use nanobodies (camelid nanobodies, or F(ab) fragments of secondary antibodies) and/or direct conjugation of DNA to a primary antibody. By combining these two options (antibody fragments or direct conjugation of DNA to primary antibodies) with the three options for DNA-antibody conjugation strategies presented above, iExM with much smaller structural errors might be possible.

Supplementary Note 5. Resolution measurement: We estimated the point spread function (PSF) of iExM by measuring the full width at half maximum (FWHM) of single microtubule sidewalls, deriving a value of 25.8 ± 7.7 nm (**Supplementary Fig. 6a**). This number was comparable to the FWHM of single microtubule sidewalls measured by other super-resolution microscopies (16-25 nm for 4Pi single-molecule switching nanoscopy (4PiSMSN) imaging of microtubules with a regular secondary antibody[4] and 21-27 nm for buffer-enhanced STORM imaging of microtubules with an antibody fragment[5]). We estimated the point spread function (PSF) of iExM independent of the labels (primary antibody and DNA-conjugated secondary antibody) by deconvolving images of microtubule sidewalls by idealized microtubules (generated according to the model of **Supplementary Fig. 3**) bearing primary antibodies and DNA-conjugated secondaries (but not modeling the blur due to optical diffraction). This yielded a value of 22.3 nm ± 5.3 nm (**Supplementary Fig. 6b**) for the contribution to the PSF due to the gelation, expansion, and optical imaging processes.

In iterative expansion microscopy, specimens are expanded 20-fold, but the microscope resolution is not improved by exactly 20-fold because the gelation and expansion process may introduce error. We can estimate the magnitude of this error by simulating (using the iExM simulator described in **Supplementary Fig. 2**, which includes optical blur due to diffraction) the FWHM of single microtubule sidewalls; we obtain 19.4 $\pm$ 1.4 nm for this FWHM, which models the case where microtubules are labeled with a primary antibody and DNA-conjugated secondary antibody and then expanded 20-fold without gel-related error (**Supplementary Fig. 6a**). Thus, the experimental PSF (25.8 nm, **Supplementary Fig. 6a**) is ~6 nm larger than the simulated value. Why is this? Before expansion, polymer chains form a dense polymer network with a mesh size of a few nanometers (small angle x-ray scattering measurements of similar gels suggest a mesh size of

Nature Methods: doi:10.1038/nmeth.4261

1-2 nm, ref. [6]). During gelation and expansion, the 5' acrydite moieties would be anchored to nearby polymer chains, which would "coarse grain" the set of possible acrydite anchoring points (since acrydites could not be anchored at a point in space unless a gel chain was present). During expansion itself, gels may not move perfectly evenly, as well. Such broadening would not greatly alter the mean peak-to-peak distance between target proteins arranged in a stereotyped complex, because the errors of 5'acrydite tags would be averaged out in the final images (**Supplementary Fig. 6c**). However, these gel effects would broaden the PSF of iExM by randomly moving 5'acrydite tags from their initial positions.

To gauge the impact of such errors on our original simulation (**Supplementary Fig. 2**), we incorporated errors of this scale into the simulation of **Supplementary Fig. 2**, by randomly moving 5' acrydites in the cylinder by 5-10 nm relative to their initial positions and performing the simulation of **Supplementary Fig. 2a** again. As shown in **Supplementary Fig. 6c**, an additional 5-10 nm positional error did not greatly alter the overall microtubule profile, shifting the peak-to-peak distance between the sidewalls by a few nanometers.

Supplementary Note 6. Expansion uniformity: Expansion uniformity across length scales of tens to hundreds of nanometers can be estimated by analyzing how the microtubule diameter varies along the long axis of the microtubule. Before expansion, this variation would be a result of two factors: variation in the actual microtubule diameter along the microtubule long axis before expansion, and variation in the thickness of the primary and secondary antibody layers along the microtubule long axis. If expansion was perfectly uniform, then the variation in the microtubule diameter along the microtubule long axis after expansion would be the pre-expansion variation, scaled up by the expansion factor. However, if the expansion was not uniform, then this variation might be larger than expected from a simple scaling.

By comparing the standard deviation of the microtubule diameter along the microtubule long axis as measured in STORM imaging vs. iExM imaging, we can calculate the nonuniformity of expansion across length scales of tens to hundreds of nanometers. The standard deviation of the peak-to-peak sidewall distances measured by STORM, over distances of 400 nm along the microtubule axis, was 4.7 nm (n = 110 from two cultures). This standard deviation was 10.3 nm (in scaled-down-to-pre-expansion units) when measured by iExM imaging of cultured cells (n = 307 from one cultures), and 10.5 nm when measured by hp-iExM imaging of cultured cells. The difference of variances between iExM and STORM ($(10.3^2 – 4.7^2)^{1/2}$ = 9.2 nm deviation) could be attributed to the extra DNA layer used in ExM but not STORM, as well as any non-uniformity of expansion. We calculated this standard deviation of post-expansion sidewall distances of microtubules in tissues, obtaining 13.5 nm for the brain (n = 96 from one samples), 11.5 nm for the lung (n = 55 from one samples), and 13.6 nm for the liver (n = 95 from one samples). The difference of variances (e.g., $(13.6^2$ nm $– 4.7^2)^{1/2}$ = 12.8 nm deviation for the liver) again would be attributed to the iExM-specific properties – the DNA layer and non-uniform expansion. It is nontrivial to precisely separate the effects of DNA layer and non-uniform expansion from these measurements and calculations.

Nature Methods: doi:10.1038/nmeth.4261

Supplementary Note 7. Discussion on the size of the linker DNA: For DNA amplification (**Supplementary Fig. 8**), the final expansion occurred in 0.2x PBS to maintain DNA hybridization, although this resulted in less expansion than distilled (DI) water. For LNA, the second gel was expanded in DI water, enabling full expansion, and made possible by the strong hybridization between LNA and DNA which survives immersion in DI water[3]. The use of a long linker DNA, and then hybridizing multiple DNA or LNA strands to the linker DNA, would not add a large error to the location of biological targets, as the DNA and LNA strands are hybridized to the linker DNA after the 2nd expansion, so that the effective positional error, calculated by dividing the positional error by the expansion factor, is negligible (for example, the length of a fully stretched 100-bp linker DNA is expected to be around 33 nm, but the effective positional error caused by this linker DNA would be only 33 / 20 ~ 1.7 nm).

Supplementary Note 8. Triple round expansion: We designed a triple expansion protocol (**Supplementary Fig. 15**) where the first swellable gel uses the disulfide-containing crosslinker N,N'-cystaminebisacrylamide (which can be cleaved with tris(2-carboxyethyl)phosphine (TCEP)), the second swellable gel uses the diol-containing crosslinker DHEBA (which can be cleaved with NaOH), and the third swellable gel uses the standard crosslinker BIS (which is resistant to both TCEP and NaOH). We expect that a challenge to using iterative expansion microscopy with a larger expansion factor (>50 fold) would be validating the nanoscale expansion uniformity. To validate 20-fold expansion, we used microtubules as molecular rulers, but even smaller structures would be required to validate the resolution of 50-fold expansion. One possible option would be DNA origami, as a wide range of DNA origami structures are available[7] and large probes (e.g., antibodies) are not required to anchor them to the gel.

Nature Methods: doi:10.1038/nmeth.4261

References

1. Weber, K., Rathke, P. C. & Osborn, M. Cytoplasmic microtubular images in glutaraldehyde-fixed tissue culture cells by electron microscopy and by immunofluorescence microscopy. *Proc. Natl. Acad. Sci.* **75,** 1820–1824 (1978).

2. Chi, Q., Wang, G. & Jiang, J. The persistence length and length per base of single-stranded DNA obtained from fluorescence correlation spectroscopy measurements using mean field theory. *Phys. A Stat. Mech. its Appl.* **392,** 1072–1079 (2013).

3. K. Singh, S., A. Koshkin, A., Wengel, J. & Nielsen, P. LNA (locked nucleic acids): synthesis and high-affinity nucleic acid recognition. *Chem. Commun.* 455–456 (1998). doi:10.1039/A708608C

4. Huang, F. *et al.* Ultra-High Resolution 3D Imaging of Whole Cells. *Cell* **166,** 1028–1040 (2017).

5. Olivier, N., Keller, D., Gönczy, P. & Manley, S. Resolution doubling in 3D-STORM imaging through improved buffers. *PLoS One* **8,** e69004 (2013).

6. Cohen, Y., Ramon, O., Kopelman, I. J. & Mizrahi, S. Characterization of inhomogeneous polyacrylamide hydrogels. *J. Polym. Sci. Part B Polym. Phys.* **30,** 1055–1067 (1992).

7. Veneziano, R. *et al.* Designer nanoscale DNA assemblies programmed from the top down. *Science (80-.).* **352,** 1534 LP-1534 (2016).

Note: This protocol has not been peer-reviewed.

Iterative expansion microscopy

Jae-Byum Chang, Fei Chen, Young-Gyu Yoon, Erica E. Jung, Hazen Babcock, Jeong Seuk Kang, Shoh Asano, Ho-Jun Suk, Nikita Pak, Paul W. Tillberg, Asmamaw Wassie, Dawen Cai, Edward S. Boyden

Media Lab and McGovern Institute, Departments of Biological Engineering and Brain and Cognitive Sciences, Massachusetts Institute of Technology (MIT), Cambridge, MA 02139

Abstract

Recently we developed iterative expansion microscopy (iExM), in which biological specimens are iteratively expanded by repeatedly embedding them in swellable hydrogels and swelling the resultant tissue-hydrogel composites. Two rounds of ~4.5x expansion result in ~4.5 x 4.5 ~20x physical magnification, enabling ~25 nm resolution imaging on conventional diffraction limited microscopes. In this protocol, we describe detailed experimental procedures starting from cultured cells or intact tissues, proceeding with immunostaining of target proteins, followed by synthesis of swellable hydrogels bearing a chemically cleavable crosslinker throughout the specimens, swelling of the gel, synthesis of a second swellable hydrogel in the space opened up by the first swelling step, swelling of the second gel, and signal amplification. This protocol has successfully been applied to cultured cells and intact tissues, enabling high precision nanoscopy on scalable, conventional diffraction-limited optics.

Introduction

We earlier showed that it is possible to physically magnify preserved biological specimens by embedding them in a densely crosslinked polyelectrolyte gel, anchoring key labels or biomolecules to the gel, mechanically homogenizing the specimen, and then swelling the gel-specimen composite by ~4.5x in linear dimension, a process we call expansion microscopy (ExM)[1–3]. The net impact is that on a conventional diffraction limited microscope with ~300 nm resolution, you can now achieve an effective resolution of ~300 / 4.5 ~ 60-70 nm. We recently developed iterative expansion microscopy (iExM), in which a sample is expanded, then a second swellable polymer mesh is formed in the space newly opened up by the first expansion, and finally the sample is expanded again (accepted, *Nature Methods*). iExM expands biological specimens ~4.5 × 4.5 or ~20x in linear dimension, and enables ~25 nm resolution imaging of cells and tissues on conventional microscopes. We have used iExM to visualize synaptic proteins, as well as the detailed architecture of dendritic spines, in mouse brain circuitry. The protocol below describes how to perform iExM. We highly recommend

Nature Methods: doi:10.1038/nmeth.4261

successful implementation of conventional ExM[1] before beginning work on iExM, since iExM shares many of the same steps, but applied in an iterative fashion.

Subject terms

Imaging, Neuroscience

Keywords

Microscopy, Super-resolution, Immunohistochemistry, Brain, Antibodies, Nanoscopy, STORM, PALM, STED, Expansion microscopy

Reagents

1. List of chemicals: sodium acrylate (here abbreviated AA, Sigma, 408220), acrylamide (AAm, Sigma, A9099), N,N′-methylenebisacrylamide (BIS, Sigma, M7279), ammonium persulfate (APS, Sigma, A3678), N,N,N′,N′-Tetramethylethylenediamine (TEMED, Sigma, T7024), 4-Hydroxy-TEMPO (H-tempo, Sigma, 176141), N,N'-(1,2-Dihydroxyethylene)bisacrylamide (DHEBA, Tokyo Chemical Industry, D2864), paraformaldehyde (Electron Microscopy Sciences, 15710), glutaraldehyde (Electron Microscopy Sciences 16020), Triton X-100 (Sigma, X100), glycine (Sigma, 50046), phosphate buffered saline 10x (PBS 10x, Life Technologies, 70011-044), dextran sulfate 50% (Millipore, S4030), saline-sodium citrate 20x (SSC 20x, Life Technologies, 15557), yeast tRNA (Roche, 10109495001), normal donkey serum (NDS, Jackson ImmunoResearch, 017-000-001), proteinase K (New England Biolabs, P8107S), ethylenediaminetetraacetic acid (EDTA, Sigma, EDS), guanidine HCl (Sigma, G3272), Tris-HCl, 1M pH 8.0 (Life Technologies, AM9855)
2. Blocking buffer: 1x PBS, 5% NDS, 0.1% Triton X-100
3. Hybridization buffer: 2x SSC, 10% dextran sulfate, 1 mg/mL yeast tRNA, 5% NDS, 0.1% Triton X-100
4. DNA hybridization buffer: 4x SSC, 20% formamide
5. Digestion buffer: 50 mM Tris pH 8.0, 1mM EDTA, 0.5% Triton X-100, 0.8 M guanidine HCl, 8 units/mL Proteinase K (1:100 dilution)
6. Pre-gel incubation solution: 8.625% AA, 2.5% AAm, 0.2% DHEBA, 1.865M sodium chloride, 1x PBS
7. 1st gel solution: 8.625% AA, 2.5% AAm, 0.2% DHEBA, 0.2% APS, 0.2% TEMED, 1.865M sodium chloride, 1x PBS, 0.01% H-tempo

8. Re-embedding solution: 10% AAm, 0.2% DHEBA, 0.05% APS, 0.05% TEMED
9. 2nd gel solution: 8.625% AA, 2.5% AAm, 0.15% BIS, 0.05% APS, 0.05% TEMED, 2M sodium chloride, 1x PBS
10. DNA & LNA:
    A. A1' 5'amine, AA CCG AAT ACA AAG CAT CAA CG with 5'amine
    B. A1 5'acrydite 3'alexa488, CG TTG ATG CTT TGT ATT CGG T with 5'acrydite 3'alexa488
    C. A1' 5'acrydite 3'atto565, CCG AAT ACA AAG CAT CAA CG with 5'acrydite 3'atto565
    D. A2' 4LNA-A1' 5'acrydite, GG TGA CAG GCA TCT CAA TCT ATT ACA AAG CAT CAA CGA TTA CAA AGC ATC AAC GAT TAC AAA GCA TCA ACG ATT ACA AAG CAT CAA CG with 5'acrydite
    E. LNA-A1 3'atto565, CGTTGATGCTTTGTA with 3'atto565 (underlined letters: LNA)

Procedure

1. Sample preparation

A. Cultured cells

i. Cells can be cultured as desired. In this protocol, we use Nunc Lab-Tek II chambered coverglasses (ThermoFisher, 155409).

ii. Wash cultured cells in 1x PBS three times at room temperature, briefly each time, before fixation.

iii. Fix cells with room temperature 4% formaldehyde in 1x PBS for 10 minutes.

iv. Wash cells with room temperature 100 mM glycine in 1x PBS three times, for 5 minutes each time.

B. Mouse tissue slices

i. Anesthetize mice using isoflurane in oxygen (or other animal care committee approved anesthetic) and perfuse with room temperature 1x PBS until the blood runs clear, then 30 mL room temperature fixative solution (4% paraformaldehyde in 1x PBS). Other fixation protocols may suffice as well (e.g., cold 4% paraformaldehyde in 1x PBS, perfused for 30 minutes, may work).

ii. Harvest organs of interest, then store them in the same fixative at 4°C for 24 hours.

iii. Slice organs on a vibratome (Leica VT1000s) to a thickness of 100 μm or 150

Nature Methods: doi:10.1038/nmeth.4261

μm, in cold 100 mM glycine in 1x PBS, then store them in 100 mM glycine in 1x PBS at 4°C until ready for staining.

2. Staining

A. Cultured cells

i. Incubate cells in blocking buffer for 10 minutes at room temperature.

ii. Incubate cells with primary antibodies in blocking buffer for one hour at room temperature and wash in 1x PBS three times for 5 minute durations each, all at room temperature.

iii. Incubate cells with DNA (e.g., A1' 5'amine)-conjugated secondary antibodies in hybridization buffer at a concentration of 10 μg/mL for one hour with gentle shaking at room temperature, then wash in 1x PBS at room temperature three times for 5 minute durations each (see http://expansionmicroscopy.org/ to find a step-by-step instruction of how to do DNA-antibody conjugation, as published in ref. [1]).

iv. Incubate cells with DNAs with 5'acrydite modification (e.g., A1 5'acrydite 3'alexa488) in hybridization buffer at a concentration of 0.5 ng/μL for one hour at room temperature with gentle shaking, then wash three times, for 5 minute durations each, in 1x PBS at room temperature.

B. Tissue slices

i. Incubate tissue slices in blocking buffer at room temperature for two hours with gentle shaking.

ii. Incubate tissue slices with primary antibodies in blocking buffer for 2-3 days at 4°C with gentle shaking and then wash in blocking buffer at room temperature with gentle shaking four times, for 30 minutes each time.

iii. Incubate tissue slices with DNA (e.g., A1' 5'amine)-conjugated secondary antibodies in hybridization buffer overnight at room temperature with gentle shaking and then wash in blocking buffer four times, at room temperature with gentle shaking, for 30 minutes each time.

iv. Incubate tissue slices with DNAs with 5' acrydite modification (e.g., A1 5'acrydite 3'alexa488) at a concentration of 1 ng/μL overnight at room temperature with gentle shaking and then wash in blocking buffer four times, at room temperature with gentle shaking, for 30 minutes each time.

3. Gelation

A. 1st gel synthesis of cultured cells

Nature Methods: doi:10.1038/nmeth.4261

i. Incubate cells in pre-gel incubation solution at 4°C overnight.

ii. Incubate cells in 1st gel solution at 4°C for 30 minutes.

iii. Replace the solution with a freshly prepared 1st gel solution and incubate at 4°C for 30 minutes, then incubate another three hours at 37°C.

iv. Add digestion buffer to culture wells, and then take gels out from the wells using a disposable spatula and incubate gels in digestion buffer overnight at room temperature with gentle shaking.

v. Incubate gels in DI water at room temperature with gentle shaking three times for 2 hours, 2 hours, and then overnight, respectively.

B. 1st gel synthesis of tissue slices

i. Incubate tissue slices in pre-gel incubation solution at 4°C overnight.

ii. Incubate tissue slices in fresh 1st gel solution, at 4°C for 30 minutes, twice.

iii. Place tissue slices, with accompanying 1st gel solution, between two pieces of #1 coverglass separated by another #1 coverglass (Fig. 1a) and then incubate at 37°C for 3 hours.

iv. Incubate gels in digestion buffer overnight at room temperature with gentle shaking.

v. Incubate gels in DI water at room temperature with gentle shaking three times, for 2 hours, 2 hours, and then overnight, respectively.

C. Re-embedding of expanded gels (both cultured cells and tissue slices)

i. Incubate gels in fresh re-embedding solution at room temperature for 30 minutes twice with gentle shaking.

ii. Place gels between two pieces of #1 coverglass (Fig. 1b), then place in a nitrogen-filled chamber, and incubate at 37°C for 1.5 hours.

iii. Remove from the nitrogen-filled chamber, and incubate gels in DNA hybridization buffer twice, at room temperature with gentle shaking, thirty minutes each time.

iv. Incubate gels with complementary DNA (A1' 5'acrydite 3'atto565) (or linker DNA A2' 4LNA-A1' 5'acrydite if signal amplification is desired) in DNA hybridization buffer at a concentration of 0.5 ng/μL (or 2 ng/μL for linker DNA) at room temperature overnight with gentle shaking and then wash in DNA hybridization buffer three times, at room temperature with gentle shaking, for 2 hours, 2 hours, and overnight respectively.

D. 2nd gel synthesis (both cultured cells and tissue slices)

i. Incubate gels in fresh 2nd gel solution at room temperature for 30 minutes twice

Nature Methods: doi:10.1038/nmeth.4261

with gentle shaking.

ii. Place gels between two pieces of #1 coverglass (Fig. 1b) and then place in a nitrogen-filled chamber, and incubate at 37°C for 1.5 hours.

iii. Remove from the nitrogen-filled chamber, and incubate gels in 0.2M sodium hydroxide, at room temperature with gentle shaking, for 1 hour.

iv. For gels that will not undergo signal amplification, incubate gels in DI water three times, at room temperature with gentle shaking, for 2 hours, 2 hours, and overnight, respectively.

v. For gels that will undergo signal amplification, incubate gels in DNA hybridization buffer twice, for thirty minutes each time, at room temperature with gentle shaking, and then incubate gels with LNA (LNA-A1 3'atto565) in DNA hybridization buffer at a concentration of 0.5 ng/μL at room temperature with gentle shaking for overnight, then wash in DNA hybridization buffer at room temperature with gentle shaking three times, for 2 hours, 2 hours, and overnight, respectively. Incubate gels in DI water at room temperature with gentle shaking, three times, for 2 hours, 2 hours, and overnight, respectively.

Figure

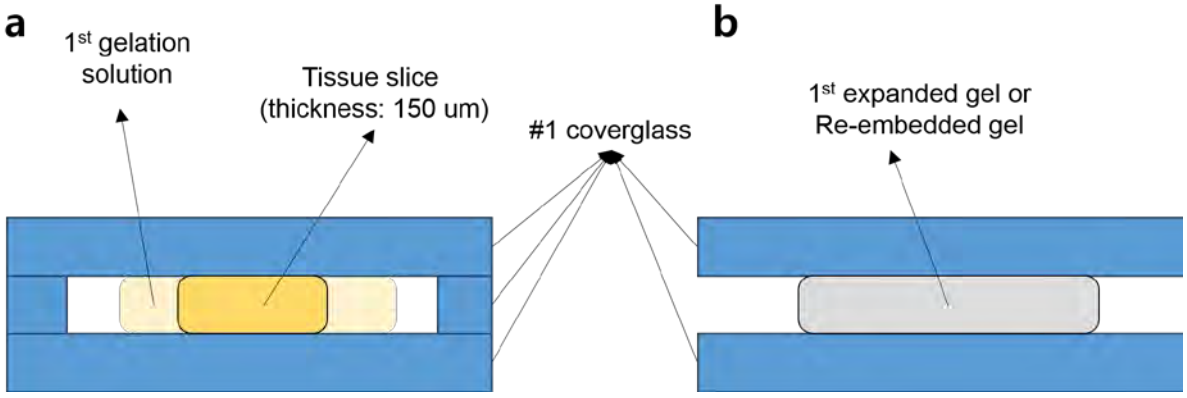

Figure 1. Assembly of gelation apparatus. (a) Gelation apparatus for 1st swellable gel synthesis, for tissue slices. (b) Gelation apparatus for re-embedding and 2nd swellable gel synthesis, for tissue slices and cultured cells.

Troubleshooting

If gels do not form, check the color of the sodium acrylate-containing solution. We make a 33% (w/w) sodium acrylate stock solution and use it to make the final gel solutions. The sodium acrylate stock solution should be colorless (or slightly yellow), but not very yellow – if very yellow, that means the sodium acrylate has gone bad. We recommend storing sodium acrylate

Nature Methods: doi:10.1038/nmeth.4261

powder at -20°C.

References

1. Chen, F., Tillberg, P. W. & Boyden, E. S. Expansion microscopy. *Science (80-.).* **347,** 543–548 (2015).
2. Tillberg, P. W. *et al.* Protein-retention expansion microscopy of cells and tissues labeled using standard fluorescent proteins and antibodies. *Nat. Biotechnol.* **34,** 987–992 (2016).
3. Chen, F. *et al.* Nanoscale imaging of RNA with expansion microscopy. *Nat. Methods* **13,** 679–684 (2016).

Associated publications

Iterative expansion microscopy

Jae-Byum Chang, Fei Chen, Young-Gyu Yoon, Erica E. Jung, Hazen Babcock, Jeong Seuk Kang, Shoh Asano, Ho-Jun Suk, Nikita Pak, Paul W. Tillberg, Asmamaw Wassie, Dawen Cai, Edward S. Boyden, Nature Methods

Author Information

Affiliations

Media Lab, Massachusetts Institute of Technology (MIT), Cambridge, MA, USA
Jae-Byum Chang, Young-Gyu Yoon, Erica E. Jung, Shoh Asano, Edward S. Boyden

Department of Biomedical Engineering, Sungkyunkwan University, Seoul, Korea
Jae-Byum Chang

Department of Biological Engineering, MIT, Cambridge, MA, USA
Fei Chen, Asmamaw Wassie, Edward S. Boyden

Department of Electrical Engineering and Computer Science, MIT, Cambridge, MA, USA
Young-Gyu Yoon, Paul W. Tillberg

Harvard Center for Advanced Imaging, Harvard University, Cambridge, MA, USA
Hazen Babcock

Applied Physics, Harvard University, Cambridge, MA, USA
Jeong Seuk Kang

Health Sciences and Technology, MIT, Cambridge, MA, USA
Ho-Jun Suk

Department of Mechanical Engineering, MIT, Cambridge, MA, USA

Nikita Pak

Department of Cell and Developmental Biology, University of Michigan, Ann Arbor, MI, USA
Dawen Cai

McGovern Institute, MIT, Cambridge, MA, USA
Edward S. Boyden

Department of Brain and Cognitive Sciences, MIT, Cambridge, MA, USA
Edward S. Boyden

Corresponding author

Correspondence should be addressed to E.S.B (esb@media.mit.edu)

Competing financial interests

E.S.B., J.-B.C., F.C., and P.W.T. have applied for a patent on iExM. E.S.B. is co-founder of a company, Expansion Technologies, that aims to provide expansion microscopy kits and services to the community.

Nature Methods: doi:10.1038/nmeth.4261